MEASUREMENT OF IGNITION TIME ON THERMALLY THIN MATERIAL ASSEMBLIES UNDER CONVECTIVE AND RADIATIVE HEATING

A THESIS

Presented to

The Faculty of the Division

of Graduate Studies

By

Robert Paul Lowery

In Partial Fulfillment

of the Requirements for the Degree

Master of Science in Mechanical Engineering

Georgia Institute of Technology

February, 1977

MEASUREMENT OF IGNITION TIME ON THERMALLY THIN MATERIAL ASSEMBLIES UNDER CONVECTIVE AND RADIATIVE HEATING

Approved:

P. Durbetaki, Chairman

G. T. Colwell

W. C. Tincher

Date approved by Chairman: 3/8/1977

ACKNOWLEDGMENTS

I would like to thank my thesis advisor, Dr. Pandeli Durbetaki, for his help, interest, and the valuable suggestions and criticisms throughout the duration of this investigation. Thanks are due to Dr. W. C. Tincher and Dr. G. T. Colwell, of the thesis reading committee, for their constructive comments about this thesis.

I would also like to thank the National Science Foundation for its support during the investigation.

I wish to thank Jack Tingle and Vinton Wolfe for their advice and friendship during this research. And finally, I express my appreciation to my wife, Kathy, for her understanding and encouragement.

TABLE OF CONTENTS

Chapter Page

LIST OF TABLES

LIST OF ILLUSTRATIONS

NOMENCLATURE

A	frequency factor
$B_i, \underset{\sim}{B}$	forcing vector, equation (4.56)
b_{ij}	polynomial coefficients for lateral profiles, equation (4.41)
C_{ij}	coefficient matrix, equation (4.56)
c	specific heat of solid
c_p	specific heat at constant pressure
D	mass diffusion coefficient
E	activation energy
e	emmissivity
F	shape factor
G	interfabric spacing
g	acceleration due to gravity
H	boundary layer thickness at top of heated surface, $h_m(L)$
$h(x)$	local boundary layer thickness
h	convective film coefficient
i	specific enthalpy
Δi_f	specific enthalpy of formation
k	thermal conductivity
L	heated vertical length
$\dot{m}$	mass flow rate
$\bar{m}$	exponent for streamwise velocity profile, equation (4.40)

N_{Gr}	Grashof number
N_{Pr}	Prandtl number
N_{Re}	Reynolds number
N_{Sc}	Schmidt number
n	order of reaction
$\bar{n}$	exponent for stream-wise boundary layer thickness profile, equation (4.40)
P(E/U)	exposure probability for given garmet use
P(I/E)	ignition probability for given exposure
P(I/U)	ignition probability for given garment use
$P_{ij}(\underset{\sim}{Y})$	profile integrals, Table 4
p	pressure
$Q_{ij}(\underset{\sim}{Y})$	equation (4.47)
q''_y	y-component of conductive heat flux, equation (4.16), (4.17)
$q''_{r,y}$	y-component of radiative heat flux, equation (4.19)
r'''	volumetric pyrolysate production rate, equation (4.3)
R	gas constant
s	wall shear equation (4.14), (4.15)
s*	normalized wall shear, equation (4.48)
T	absolute temperature
U	maximum stream-wise velocity component, $u_m(L)$
u	velocity component along x-coordinate
v	velocity component along y-coordinate
W	radiative power flux
w	mass fraction

w_f	pyrolysate concentration
w_{fl}	lower limit of ignitable pyrolysate concentration
w_{fu}	upper limit of ignitable pyrolysate concentration
x,y	rectangular coordinates
Y_1 through Y_{11}	system state variables, equation (4.20) through equation (4.30)
$\underset{\sim}{Y}$	eleven dimensional vector of $(Y_1,\ldots,Y_{11})$
$\tilde{\alpha}$	radiative absorbtivity
$\tilde{\alpha}^*$	proportionality constant, equation (4.1a)
β	coefficient of thermal expansion
δ	fabric thickness
ε	decomposable fraction of original mass
η	normalized boundary layer thickness, equation (4.33)
Λ	ignition criteria, equation (4.64)
λ	fraction of decomposable mass which evolves from the surface
μ	dynamic viscosity
ν	kinematic viscosity
ξ	normalized stream-wise component, equation (4.32)
π_{1-14}	boundary layer parameters, Table 3
π_{100}-π_{116}	front fabric parameters, Table 5
π_{200}-π_{216}	back fabric parameters, Table 6
ρ	density
$\Delta\rho$	density of decomposable mass
$\tilde{\rho}$	reflectance

$\rho\delta$	specific mass
σ	Stefan-Boltzmann constant
τ, τ^*, τ_{ref}	time, normalized time, reference time, equation (4.31)
$\tilde{\tau}$	transmissivity
ψ	profile functions for boundary layer, equations (4.35) to (4.37)

Subscripts

a	air
d	destruction time
en	endothermic reaction
ex	exothermic reaction
f	fuel, pyrolysate
G	interfabric spacing
i,j	counting indices
ig	ignition
k	counting index
L	characteristic length
md	moisture desorption
min	minimum necessary
mix	mixture
o	initial
r	radiative, reference
ref	reference
y	y-direction
1	front fabric
2	back fabric

3	gaseous region
∞	environmental temperature

Superscripts

-	averaged values
*	normalized value

SUMMARY

The Fire Hazard and Combustion Research Laboratory of the School of Mechanical Engineering at Georgia Institute of Technology has been engaged in a research program concerned with the flammability and fire hazard of thermally thin and thick materials. The present combined experimental and analytical study is a part of this research program and its objective has been to investigate the effect of chemical and thermal interaction in thermally thin pyrolyzing assemblies on the ignition time of the solid exposed to the heating source.

The investigation was divided into two parts. The first part was concerned with the measurement of ignition time on fabric assemblies exposed to a time invariant, normal flame impingement convective heat source, using the Convective Ignition Time Apparatus (CITA). Five different fabric pairs at three different spacings were exposed to a high and a low intensity of the heat source. The ignition time of the front fabric (fabric exposed to the heat source) proved to be independent of the presence of a rear fabric.

The second part of the investigation was the ignition time measurement on vertically oriented fabric assemblies exposed to a time invariant radiative heat flux, using the Radiative Ignition Time Apparatus (RITA). This phase of the

work represents an extension of earlier studies where the ignition time measurements on one similar and one dissimilar pair of fabrics at three different fabric spacings and radiative heat intensities from 6.5-14.3 W/cm^2 were carried out. The previous work was extended to include six fabric gaps and one similar and two dissimilar fabric pairs. The experimental results show that the front fabric in the assembly has a shorter ignition time than the corresponding single fabric under identical exposure conditions. Only thermal interaction between the two decomposing fabrics has been observed. There was no evidence of chemical interaction between the decomposing fabrics.

The existing model for radiative heating was modified to include the ignition of the pyrolysate gases in the boundary layer as the ignition criterion. This model was used to predict the ignition time of the front fabric. The model predicted ignition times that followed the same general trend that was seen in the experimental results. The differences between the experimental and predicted ignition times are considered to be due to the uncertainties in the chemical kinetic values, fabric properties and predicted convective film coefficients.

This work was supported by National Science Foundation Grant No. AEN72-03359 A04.

CHAPTER I

INTRODUCTION

1.1. Relevance of Fabric Flammability Research

The United States of America outranks all major industrialized nations in per capita deaths, injuries and property loss resulting from accidental fires. These fires claim the lives of 12,000 Americans each year and inflict property damage and related losses that costs the United States an estimated $11.4 billion per year [1]. Garments which ignite and injure the consumer contribute greatly to this loss. Each year 3,000 to 5,000 deaths are due to burning fabrics, and more than half of the total burn injuries result from this source [2].

In response to this problem, Congress enacted the Flammable Fabrics Act of 1953 (and further amended it in 1967) directing the Secretary of Commerce to establish reasonable safety criteria to protect the public from excessive hazards of fabric related burn injuries. This research will ultimately help in the establishment of standards which will hopefully result in a reduction of the overall fire hazard.

1.2. Previous Accomplishments

In order to establish the technical and scientific foundation for the required legislation, the Government-

Industry Research Committee on Fabric Flammability (GIRCFF) was formed whose members represented the National Science Foundation, the National Bureau of Standards, the American Textile Manufacturers Association, the Cotton Council of America, and the Man-Made Fiber Producers Association.

The principal connection between burn injury hazard and the deterministic processes leading to burn injury were established in Reference [3]. The relationship is based on the quantitative assessment of hazards in terms of accident probability, and the dependence of accident probability on the probabilities associated with all conceivable events occurring between the production of the fabric and the accidental burn injury. The probability of fabric ignition for a given exposure P(I/E) was shown [4] to be the ratio of the time it takes a fabric to ignite under given exposure conditions, called the ignition time, over the time the fabric is exposed to a given ignition source, that is, the exposure time. The overall hazard may be expressed by

$$P(B/U) = P(E/U) \cdot P(I/E) \cdot P(B/I) \qquad (1.1)$$

that is, the probability of burn injury given the intended usage is specified by the probabilities of exposure given usage, ignition given exposure, and burn injury given ignition.

Research on fabric flammability has been directed

towards the assessment of the overall garment fire hazard. Four separate research groups were selected to study the phenomena of ignition, preignition heat transfer, propagation of flame, and the assessment of burn injury. These were the Georgia Institute of Technology, the Gillette Research Institute, the Massachusetts Institute of Technology, and Factory Mutual Research Corporation.

The ignition of fabrics was studied at the Fire Hazard and Combustion Research Laboratories of the School of Mechanical Engineering at the Georgia Institute of Technology. Fabric ignition times were determined for fabric samples exposed to a heat flux for both convective and radiative heating. Comparison between analysis and experimentally determined ignition times indicate the significance of pyrolysis in delaying predicted ignition times by a factor of two to three.

1.3. Further Advances Required

The determination of the relationship between fabric behavior in a laboratory test and the hazard it represents in actual use is the central problem in the development of rational safety standards [5]. Extensive studies have been made on the ignition of single fabrics exposed to an ignition source [6,7]. Acree [8] extended the ignition studies to include the radiative heating of multi-layer assemblies and the edge impingement of a gas flame.

Additional studies on multilayer assemblies are needed

to further define the interaction between the fabric layers. Acree worked with one similar and one dissimilar pair of fabrics. Fabric spacings of 0.0, .16 and .32 cm were used with four different heating intensities. Greater fabric spacings must be used to fully determine the effect of air gap on the ignition time of the front fabric.

There has been work done by Miller [9] which suggests that there is chemical interaction between dissimilar decomposing fabric assemblies. Another dissimilar pair of fabrics should be used to determine the effect of the chemical interaction between the fabrics on the ignition time of the exposed front fabric.

The previous work on multilayer assemblies had only been concerned with radiative heating. Work is needed on the interaction between fabric layers exposed to a convective heating source.

The mathematical description of preignition processes and particularly the reliable prediction of ignition time are essential, not only for explaining fundamental combustion mechanisms but also for the rational assessment of fire hazards [10,11]. Extensive review papers by Stewart [12], Kanury [13], Merzhanov and Averson [14] reveal that previous ignition models are almost exclusively based on analysis of inert heating, allowing at most for thermal effects from an Arrhenius-type degradation.

Acree developed an analytical model for fabric

assemblies exposed to radiative heating. His ignition model took into account the effects of moisture desorption, endothermic pyrolysis and exothermic combustion of the front and back fabrics. Ignition was considered to occur when the average solid temperature reached a specified temperature, called the ignition temperature. Many other criteria have been proposed and a list can be found in Reference [15].

When a fabric is radiantly heated, an endothermic reaction associated with pyrolysis takes place. Volatiles leave the surface of the fabric and flow upwards due to buoyancy and mix with the surrounding air. Ignition has been shown to occur within this stream at some distance away from the surface [12]. This leads to the conclusion that ignition occurs in the boundary layer pyrolysate-air mixture at the concentration-dependent minimum temperature. In view of this fact, Wulff [16] defined an ignition criterion that involves the state of the pyrolysate-air mixture at ignition.

Wulff developed an ignition model for a single fabric exposed to radiative heating, using his gas phase ignition criterion. There is a need to extend the gas phase ignition criterion to the study of ignition of fabric assemblies under radiative heating.

1.4. Research Objectives

The main objective of this thesis is to assess the effect of thermal and chemical interaction on the ignition time of the front fabric of a fabric assembly. Parameters to

be studied include the effect of fabric spacing and the heating intensity. Both a convective and a radiative heat source will be used.

A second objective is to apply a new ignition criterion which accounts for the ignition of the pyrolysate gases in the boundary layer. This model will be used to predict the ignition time of the front fabric and the results will be compared with experimental measurements.

CHAPTER II

MULTI-LAYER FABRIC INTERACTION UNDER CONVECTIVE HEATING

2.1. Experimental Measurements

The purpose of the ignition time tests is to measure the destruction (ignition or melting) time of fabric assemblies exposed to a gas flame convective heat source. An apparatus was required to expose a fabric assembly to a constant intensity heat flux with instrumentation capable of detecting ignition and measuring the ignition time.

2.1.1. Apparatus and Instrumentation

The Convective Ignition Time Apparatus (CITA) was used to expose 6.35 cm diameter fabric samples to a gas flame convective heat source. This apparatus has been used in previous ignition studies, and complete details of this equipment are available in References [7,17,18].

The apparatus consists of a water cooled double-action shutter system for the rapid exposure of the sample to the premixed gas burner, a superstructure to support the sample holder, an ignition detection system and the necessary instrumentation for shutter control and timing. The apparatus is shown in Figure 1.

Existing fabric holders were used for the fabric

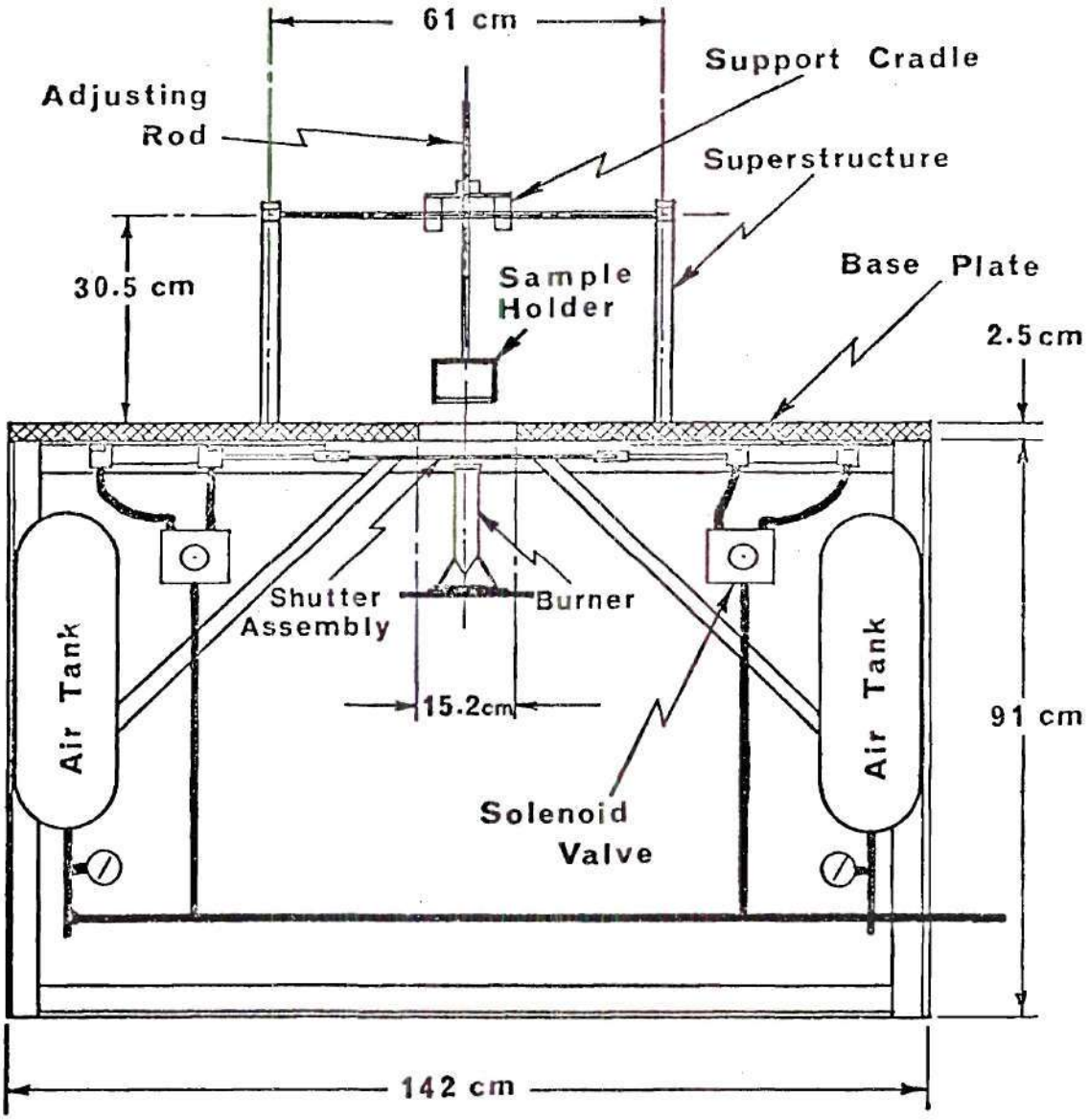

Figure 1. Schematic View of the Convective Ignition Time Apparatus (CITA)

assembly ignition tests. Aluminum spacing rings were fabricated to separate the fabric layers and were 0.16 cm, 0.32 cm and 0.64 cm. Pieces of masonite 7 cm in diameter and 0.5 cm thick were fabricated to be used as a nonporous back. A spacing ring and holder are shown in Figure 2.

The response of the front fabric was detected by an infrared detector, Model Mark I infrascope by Barnes Engineering, and was recorded by a Textronic dual beam oscilloscope, Model number 502A, on Polaroid film. The placement of the infrascope is shown in Figure 3.

Testing procedures used in the measurement of ignition and melting times are discussed in the next section.

2.1.2. Experimental Procedures

Fabric specimens were prepared from material selected and furnished by the GIRCFF. The samples were cut from large sheets by means of a circular die which yielded cleanly cut samples of appropriate size for the fabric holder. The samples were stored in the desiccated chamber for a minimum period of 24 hours prior to testing to insure a moisture content of less than eight percent.

The preconditioned fabric pair was placed in a clean fabric holder, separated by the appropriate spacing ring. The fabric holder was then placed in the sample holder in the superstructure and the burner was placed underneath the shutter. All tests were conducted with the fabric center placed 10.5 cm above the top of the 37 mm diameter burner. A low and a

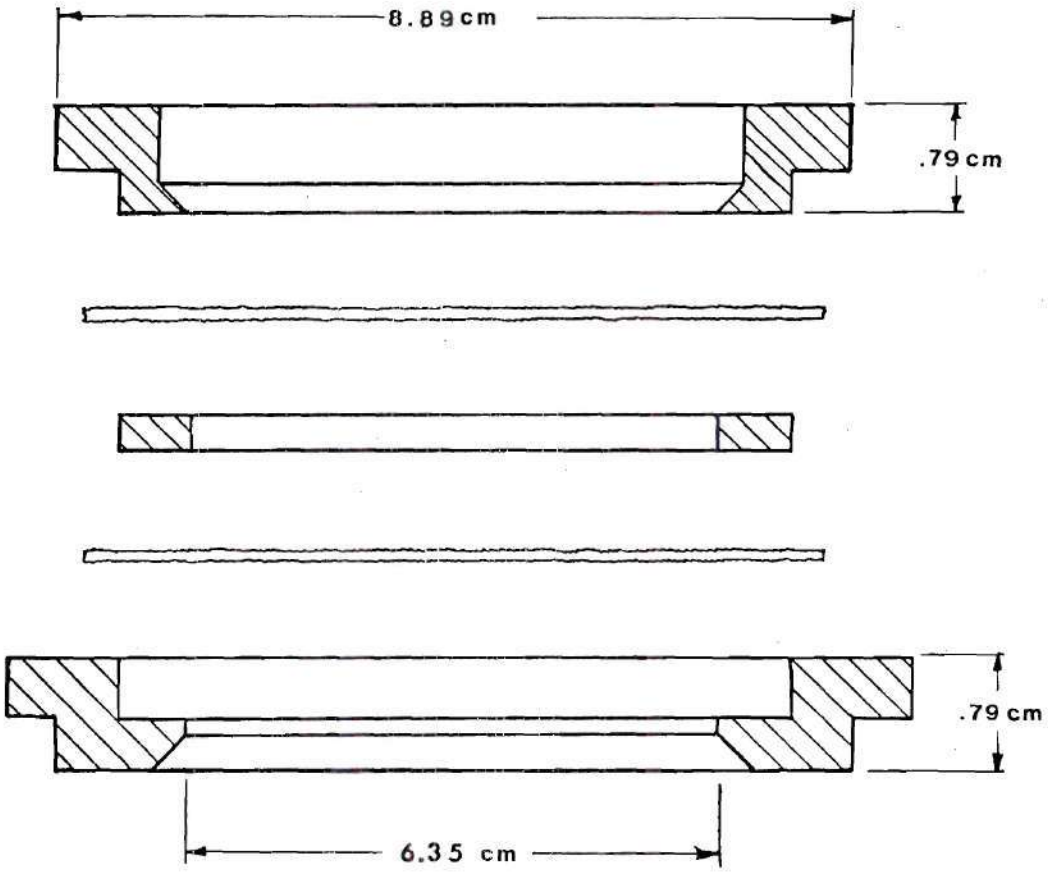

Figure 2. Cross Sectional View of the Fabric Assembly Holder

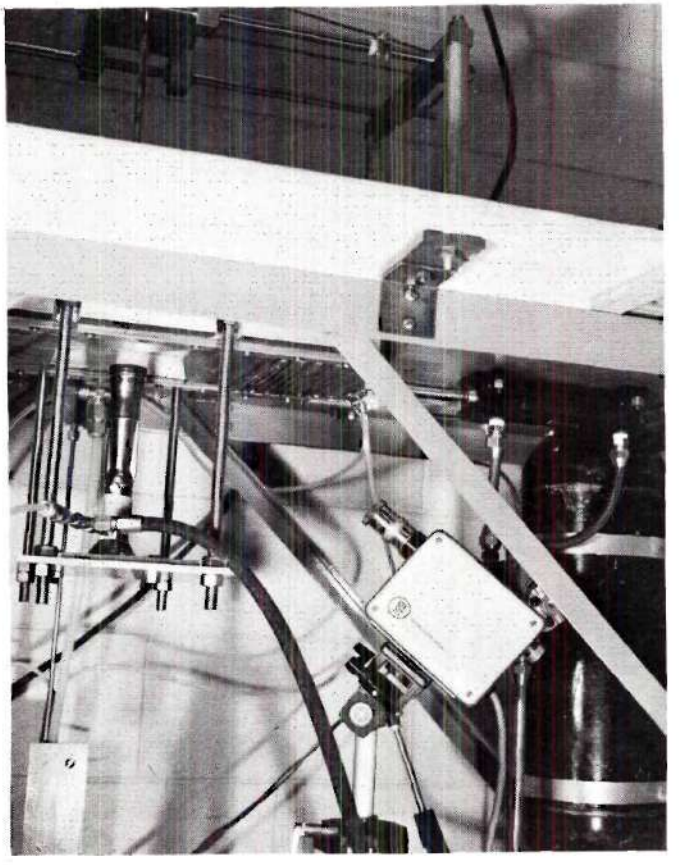

Figure 3. Lower Structure of CITA with Burner in Position and Infrared Detector

high intensity flame were used. The low convective heat flux was characterized by a combustible mixture flow rate $\dot{m}_{mix}$ = 0.36 g/s and an average flame temperature at the fabric plane T_f = 1268°K. The high convective heat flux had a flow rate $\dot{m}_{mix}$ = 0.82 g/s and flame temperature T_f = 1530°K. The equivalence ratio ϕ for the methane-air mixture is held constant at 0.86 for all tests to establish a constant composition gas stream [19].

The shutter was opened, exposing the fabric assembly to the gas flame. As the shutter opened, a microswitch was tripped which started the sweep of the oscilloscope. The trace made by the oscilloscope was recorded on Polaroid film.

2.1.3. Data Reduction and Results

Two types of ignition were observed, pyrolysate and solid ignition. The first was the ignition of the evolving pyrolysate gases. As the fabric was heated, combustible pyrolysate gases would evolve and mix with air, forming a combustible mixture. At some point in time, the pyrolysate concentration and temperature in the boundary layer were such that ignition occurred. The occurrence of pyrolysate ignition was visually observed by the presence of a blue flame. Solid ignition occured when the heat generation from exothermal reactions balanced heat losses from the fabric and from endothermic pyrolysis.

Destruction times were obtained from the oscilloscope traces of infrascope emf. Ignition tests recorded the heating

history of the front fabric. The pyrolysate ignition times were determined from the midpoint of the pyrolysate region which was the region following the inert heating period. The solid phase ignition times were determined from the intercept of the tangents of the pyrolysate region and the exponential use due to the onset of combustion. Melting times were determined from the intercepts of the tangents of the inert heating period and the sudden rise in transmitted flux due to the melt through of the fabric. Destruction time was determined as the ignition or melt through of either front or rear fabrics, and for the combinations tested, was that of the front fabric. Sample oscilloscope traces are shown in Figure A1 of the Appendix.

A total of 103 tests were conducted using CITA to determine the interaction of two parallel fabric layers. Tests were designed to examine the effects of heating intensity, inter-fabric spacing, and fabric porosity. A high and a low heating intensity were used. Fabric spacings were set at 0.0, .16 and 1.11 cm. Table 1 shows the results of the tests.

Fabrics 1 and 17 were chosen for the front fabrics because of their difference in porosity with fabrics 1 and 3 for the back fabrics. The properties of fabric 1, 3 and 17 can be found in Tables A1, A3 and A5, respectively. A piece of masonite was also used to simulate a completely nonporous back fabric. Each front fabric was tested with the same back

fabrics, number 3 and number 1 and the nonporous back. This was done to establish any effect of the fabric porosity on ignition time.

2.4. Discussion of Results

Tables 1 and 2 show that the solid ignition time of the front fabric is independent of the gap and/or the back fabric. For example, the front fabric number 1 and rear fabric number 3 combination exposed to the high intensity heat flux has an ignition time that is essentially the same as that of fabric number 1 by itself. The gap has no effect on ignition time. The same trend is seen in the other fabric combinations.

No ignition times are given for fabric number 17--nonporous back and fabric number 1--nonporous back combinations at 0.0 gap because the fabric was literally blown against the nonporous back by the jet flame.

The results indicate that the ignition time of the front fabric in fabric assemblies exposed to a convective heat flux is independent of the presence of the rear fabric.

Table 1. Summary of Fabric Assembly Ignition Tests Under Convective Heating (GIRCFF Fabric Number 17 Front)

GIRCFF Fabric No.		Ignition[1]	Ignition Time, τ_{ig}							
			High Intensity[2]				Low Intensity[3]			
			Interfabric Spacing				Interfabric Spacing			
			0.0 cm	0.16 cm	1.11 cm	Single[4]	0.0 cm	0.16 cm	1.11 cm	Single[4]
F	B		s	s	s	s	s	s	s	s
17	1	P	1.3	0.9	1.2	1.0	1.7	2.0	1.7	1.6
		S	2.1	2.0	2.1	2.0	3.1	3.2	3.2	3.0
17	3	P	1.0	1.0	1.0	1.0	1.6	1.5	1.6	1.6
		S	2.1	2.4	2.2	2.0	2.8	3.0	3.0	3.0
17	NPB[5]	P	--[6]	1.2	1.2	1.0	--[6]	1.9	1.9	1.6
		S	--[6]	2.4	2.2	2.0	--[6]	3.2	3.1	3.0

[1] P = Pyrolysate Ignition
S = Solid Ignition

[2] High Intensity
$\dot{m}_{mix}$ = 0.82 g/s, T_f = 1530°K

[3] Low Intensity
$\dot{m}_{mix}$ = 0.36 g/s, T_f = 1268°K

[4] Ignition time of single front fabric

[5] NPB = nonporous back

[6] Fabric did not ignite

Table 2. Summary of Fabric Assembly Ignition Tests Under Convective Heating (GIRCFF Fabric Number 1 Front)

GIRCFF Fabric No.			Ignition Time, τ_{ig}							
			High Intensity[2]				Low Intensity[3]			
			Interfabric Spacing				Interfabric Spacing			
F	B	Ignition[1]	0.0 cm	0.16 cm	1.11 cm	Single[4]	0.0 cm	0.16 cm	1.11 cm	Single[4]
			s	s	s	s	s	s	s	s
1	1	P	2.8	2.8	2.8	2.8	4.2	4.2	4.0	4.2
		S	5.8	6.3	6.3	6.2	9.2	9.2	9.0	8.8
1	3	P	2.4	3.0	2.6	2.8	4.2	4.1	4.3	4.2
		S	6.4	6.4	6.6	6.2	9.2	9.4	9.1	8.8
1	NPB[5]	P	--[6]	3.0	2.8	2.8	--[6]	4.8	5.0	4.2
		S	--[6]	6.4	6.4	6.2	--[6]	10.0	9.8	8.8

[1] P = Pyrolysate Ignition
S = Solid Ignition

[2] High Intensity
$\dot{m}_{mix}$ = 0.82 g/s, T_f = 1530°K

[3] Low Intensity
$\dot{m}_{mix}$ = 0.36 g/s, T_f = 1268°K

[4] Ignition time of single front fabric

[5] NPB = nonporous back

[6] Fabric did not ignite

CHAPTER III

EXPERIMENTAL MEASUREMENT OF MULTI-LAYER INTERACTION UNDER RADIATIVE HEATING

The objective of this part of the investigation is the ignition time measurement on vertically oriented fabric assemblies exposed to a radiative heat flux, using the Radiative Ignition Time Apparatus (RITA). The ignition times of the front fabric of the fabric assembly will be compared with the ignition time of a single front fabric under identical exposure conditions. The effects of thermal and chemical interaction between the two fabrics in the fabric assembly will be investigated.

3.1. Apparatus and Instrumentation

RITA was used to expose 2.54 cm diameter fabric samples to a variable intensity heat flux of between 6.5 and 14.3 W/cm^2. This apparatus has been used in previous ignition studies to obtain radiative ignition times on single fabrics [4,6] and fabric pairs [7,8,17]. Complete details of this equipment are available in References [4,6,8].

The apparatus consists of a radiant quartz lamp heater, Model Number 5208-5 from Research Inc. and a mechanical shutter system for the rapid exposure of the sample to the heater. Humidity and temperature of the environment were

controlled by a thermostatically and psychrometrically regulated chamber built by Environair Systems, Inc., which houses the RITA, and is shown in Figure 4. Ambient temperature and relative humidity were regulated to within ±0.2°C and ±2%, respectively. The apparatus assembly inside the environmental chamber is shown in Figure 5.

Existing fabric holders and the spacing rings of .16 cm and .32 cm thickness were used for the fabric assembly ignition tests. Additional aluminum spacing rings were fabricated to separate the fabric layers and these were .64 cm thickness. A spacing ring and holder is shown in Figure 6.

Basic operating principles were to bring the radiant heater to equilibrium temperature just prior to exposure, while keeping the fabric isolated, and then opening the shutters to suddenly and completely expose the fabric to the radiant heater. The thermal response of the system was then monitored for the occurrence of ignition or melting.

A Textronic dual beam oscilloscope, Model Number 502A, recorded the time-temperature history on Polaroid film. For igniting fabrics, the front fabric was monitored by an infrared detector, Model Mark 1 Infrascope by Barnes Engineering. The back fabric was monitored using a Temptron Infrascope Model IT-7310 also by Barnes Engineering. For melting fabrics, the response of the total system was monitored by using the Model Mark 1 Barnes infrascope. For ignition detection of the front fabric a mirror was employed, Kerr

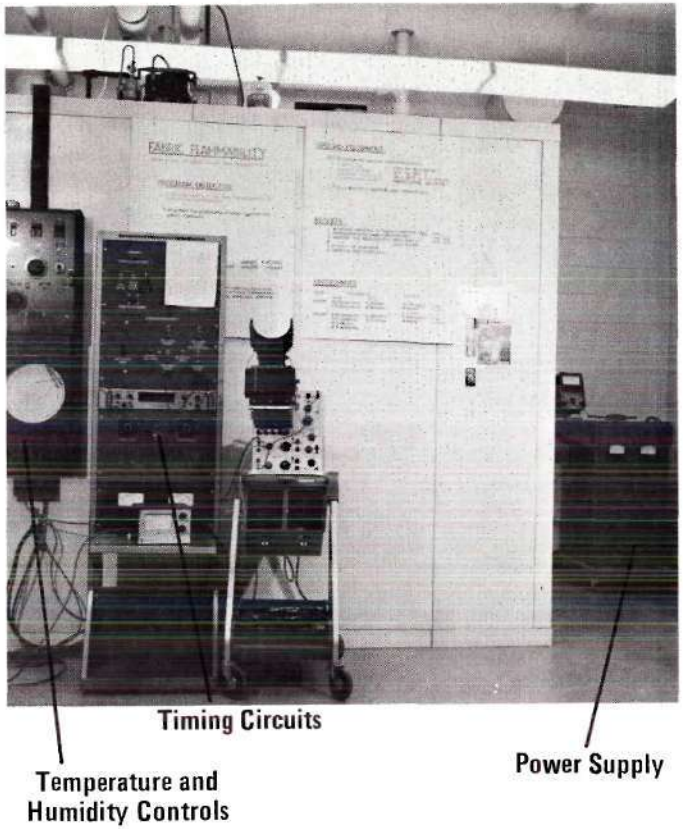

Figure 4. Environmental Chamber and Ancillary Equipment

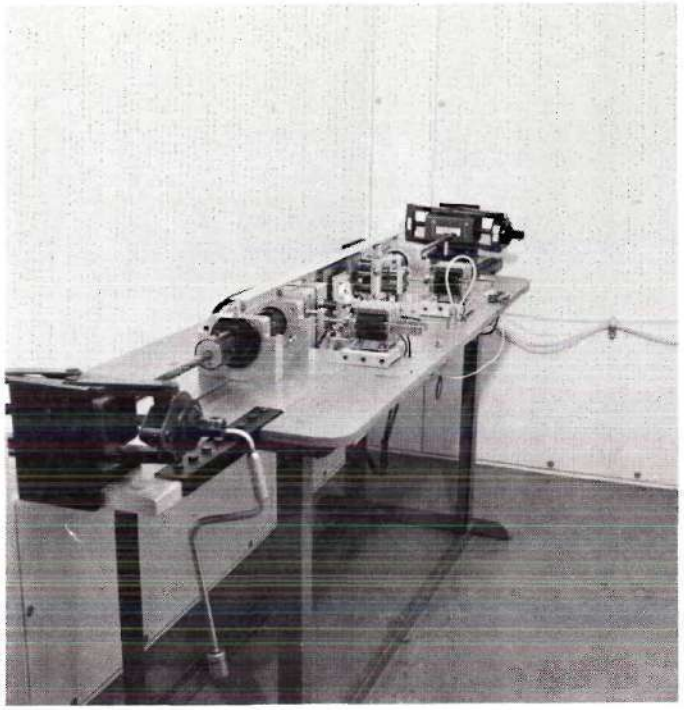

Figure 5. Radiative Ignition Time Apparatus Inside of Environmental Chamber

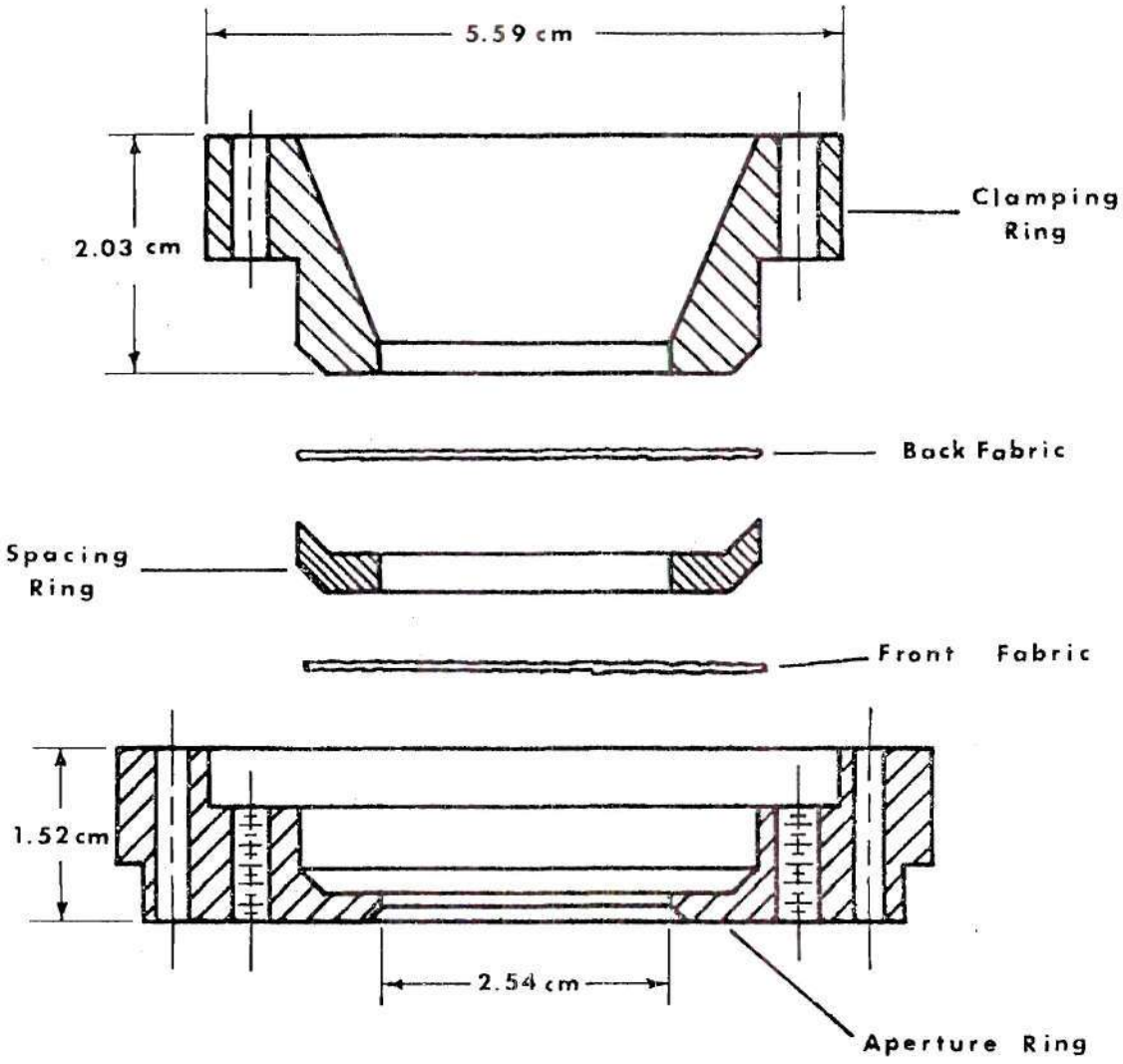

Figure 6. Cross-Sectional View of the Fabric Assembly Holder

Dental Supply Type 5C, and was supported near the front surface. The mirror and infrascope orientation are shown in Figures 7 and 8.

A mechanical timing mechanism controlled the preheat time for the heater. The idle heater voltage was measured by a Hewlett-Packard VTVM, Model Number 500-H. Calibration of incident heat flux and preheat time for a given voltage were obtained from Reference [4].

Testing procedures used in the measurement of ignition and melting times are discussed in the next section.

3.2. Experimental Procedure

The procedures followed in the determination of fabric destruction time consisted of the preparation and preconditioning of the fabric, and the exposure of the fabric sample to the radiant heater until the occurrence of ignition or melting. Destruction time of the igniting fabrics was determined by the occurrence of a luminous flame, whereas the melting fabrics were considered destroyed when the fabric structure decomposed and melt through occurred.

Ambient test conditions were controlled by conducting the radiative tests inside the environmental control chamber. The desired test conditions of 22°C and 30% relative humidity were set on the Honeywell control unit and maintained automatically. Chamber temperature and relative humidity were measured using wet and dry bulb thermometers.

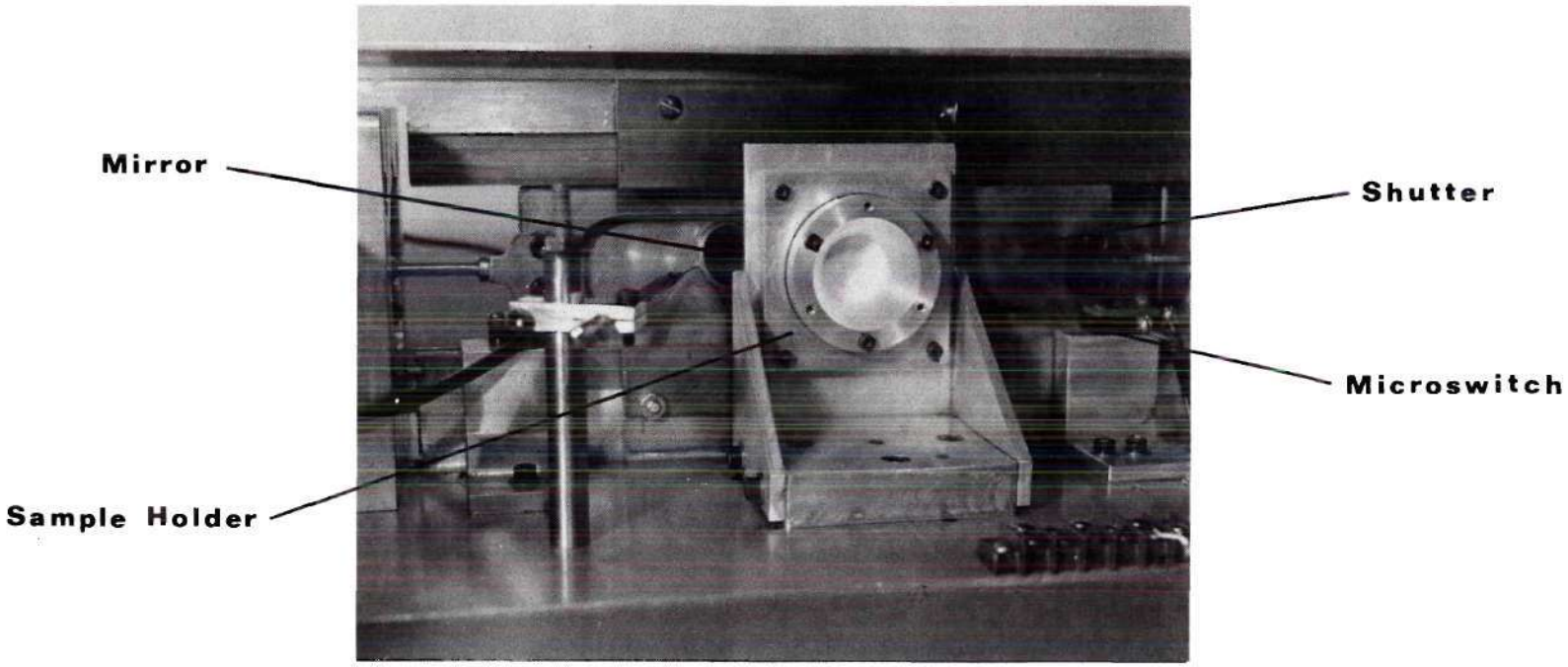

Figure 7. Experimental Arrangement for Fabric Assembly Ignition Tests

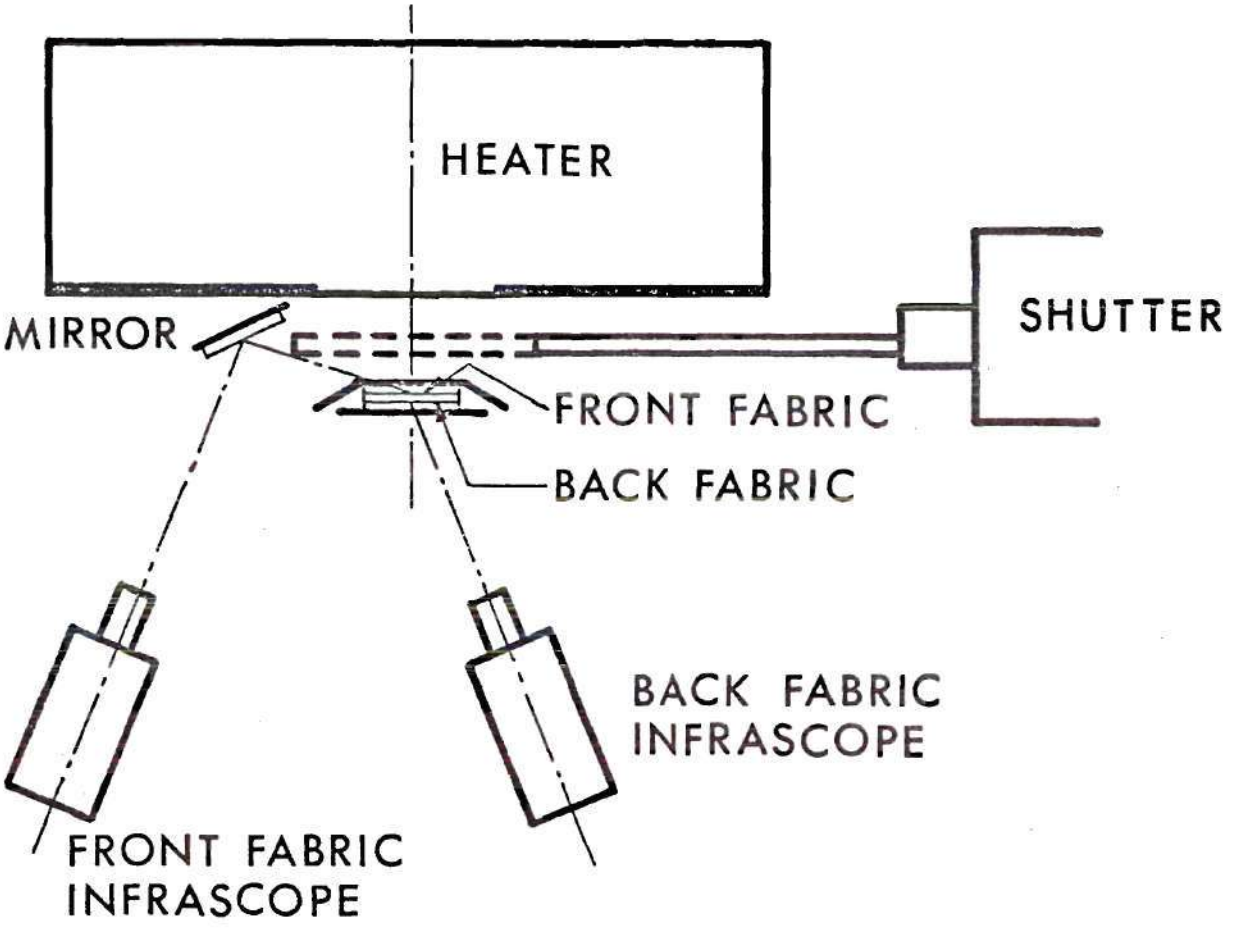

Figure 8. Schematic of Experimental Arrangement for Ignition Test on Fabric Assemblies

Fabric specimens were prepared from material selected and furnished by GIRCFF. One and one half inch (3.81 cm) diameter pieces were cut from large sheets by means of a circular die which yielded cleanly cut samples of appropriate size for the fabric holder. The samples were stored in the environmental chamber at the desired ambient testing conditions for a minimum period of 24 hours prior to testing to insure properly preconditioned moisture content and temperature.

The basic operating principles of the RITA were discussed in the previous section. The proper idle heater voltage for the desired heat flux and the proper preheat time (for the heater to reach equilibrium before shutter opening) were set. The Barnes Mark 1 infrascope was positioned and focused on the front fabric through the mirror, as shown in Figure 8. No response was obtained from the front infrascope for melting fabrics. For melting fabrics, the destruction and melt through were determined by the use of the Barnes Mark 1 infrascope located directly behind the back fabric and in line with the heater. The shutter mechanism was cocked and held in place by the release solenoid.

The preconditioned fabric pair was placed in a clean fabric holder, separated by the appropriate spacing ring, or in the case of zero gap tests, after the two fabrics had been gently pressed to insure initial contact. The fabric holder was then mounted on the holder support behind the shutter. After allowing proper warmup time for the infrascope

amplifiers and the oscilloscope, the firing sequence was started. The heater was turned on and the shutter released automatically by the timer once heater equilibrium was reached. Opening of the shutter contacted with the microswitch which in turn triggered the oscilloscope. The emf output of the infrascope detector as a function of time was then recorded on Polaroid film.

3.3. Data Reduction and Results

Destruction times were obtained from the oscilloscope traces of infrascope emf. Ignition tests recorded the heating history of the front and rear fabrics. Melting time tests recorded the transmitted flux of the heater through the assembly. Ignition times were determined from the intercept of the tangents of the inert heating region and the exponential rise due to the onset of combustion. Melting times were determined from the intercepts of the tangents of the inert heating period and the sudden rise in transmitted flux due to the melt through of the fabric. Destruction time was determined as the ignition or melt through of either front or rear fabrics, and for the combinations tested, was that of the front fabric. Sample oscilloscope traces for ignition and melting fabrics are shown in Figures A2 and A3 of the Appendix, respectively.

A total of 175 tests were conducted on the RITA to determine the interaction between fabric layers. Tests were

designed to examine the effects of variable heating intensity and variable inter-fabric spacing upon the fabric assembly destruction time.

The fabric combinations of fabric number 5 front and fabric number 5 rear, fabric number 2 front and number 5 rear, and fabric number 18 front and number 3 rear were used. The properties of fabrics 2, 3, 5 and 18 can be found in Tables A2, A3, A4 and A6 respectively. The fabric combinations of number 5 front and rear, and number 2 front and 5 rear were tested by Acree [7,8,17] with heat intensities of 6.5, 7.6, 9.25 and 13.8 W/cm^2 and gaps of 0.0, 0.159, and 0.318 cm. Acree's work was extended to include gaps of .64, 1.28 and 1.59 cm. The combination of fabric number 18 front and number 3 back was used. Intensities of 6.8, 9.0 and 14.3 W/cm^2 were used. Fabric spacing was 0.00, 0.16, 0.32, 0.64, 1.28 and 1.59 cm.

The fabric combination of fabric number 20 front and fabric number 3 back was considered as a possible combination. Preliminary testing revealed that there was no distinctive ignition point for fabric number 20.

The fabric combination of fabric number 5 front with fabric number 5 back was used to determine the effects of gap and heating intensity upon ignition time. Results of this combination are presented in Figure 9.

Tests were conducted on the combination of fabric number 2 front and fabric number 5 back and fabric number 18

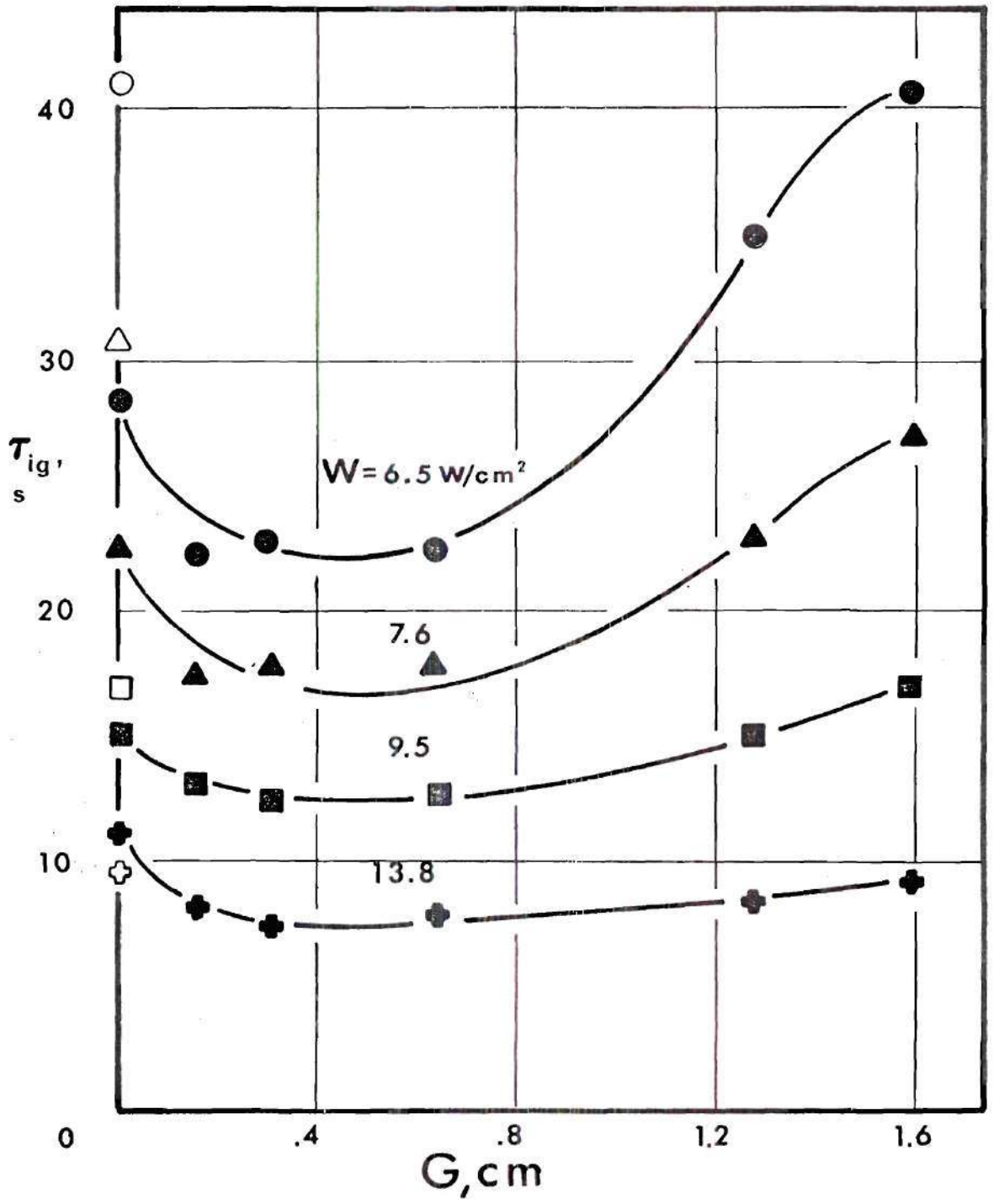

Figure 9. Ignition Time of the Front Fabric as a Function of Spacing (GIRCFF Fabric Number 5 Front and Back, Open Points Denote Single Fabric Ignition Times)

front and fabric number 3 back to determine the interaction of a synthetic and a natural fiber under radiative heating. The melting time of the front fabric for the former pair and the ignition time of the front fabric for the latter pair are shown in Figures 10 and 11, respectively.

The inside surface of some of the aluminum spacers were painted flat black. This was done to determine what effect the reflection of radiant energy off the inside surface of the spacer had on the ignition time. Tests were run with a fabric number 18 front and 3 back combination at gaps of 0.16, .32, .64, 1.28 and 1.59 cm. The results can be seen in Table 8.

3.4. Discussion of Results

Destruction time data for the front fabric is shown plotted in Figures 9 through 11. From Figure 9 it is seen that at 0.0 cm gap, for all intensities of 9.5 W/cm^2 and less, the ignition time for the single fabric is greater than that for fabric assemblies. As the intensity increases from 6.5 W/cm^2 to 9.5 W/cm^2, the time difference between the single fabric and the 0.0 cm gap decreases. At 13.8 W/cm^2, the ignition time for the 0.0 cm gap is greater than the time for the single fabric.

For the combination of fabric number 18 front and number 3 back shown in Figure 10, the same trend is seen. For intensities of 6.8 and 9.0 W/cm^2 the ignition times are

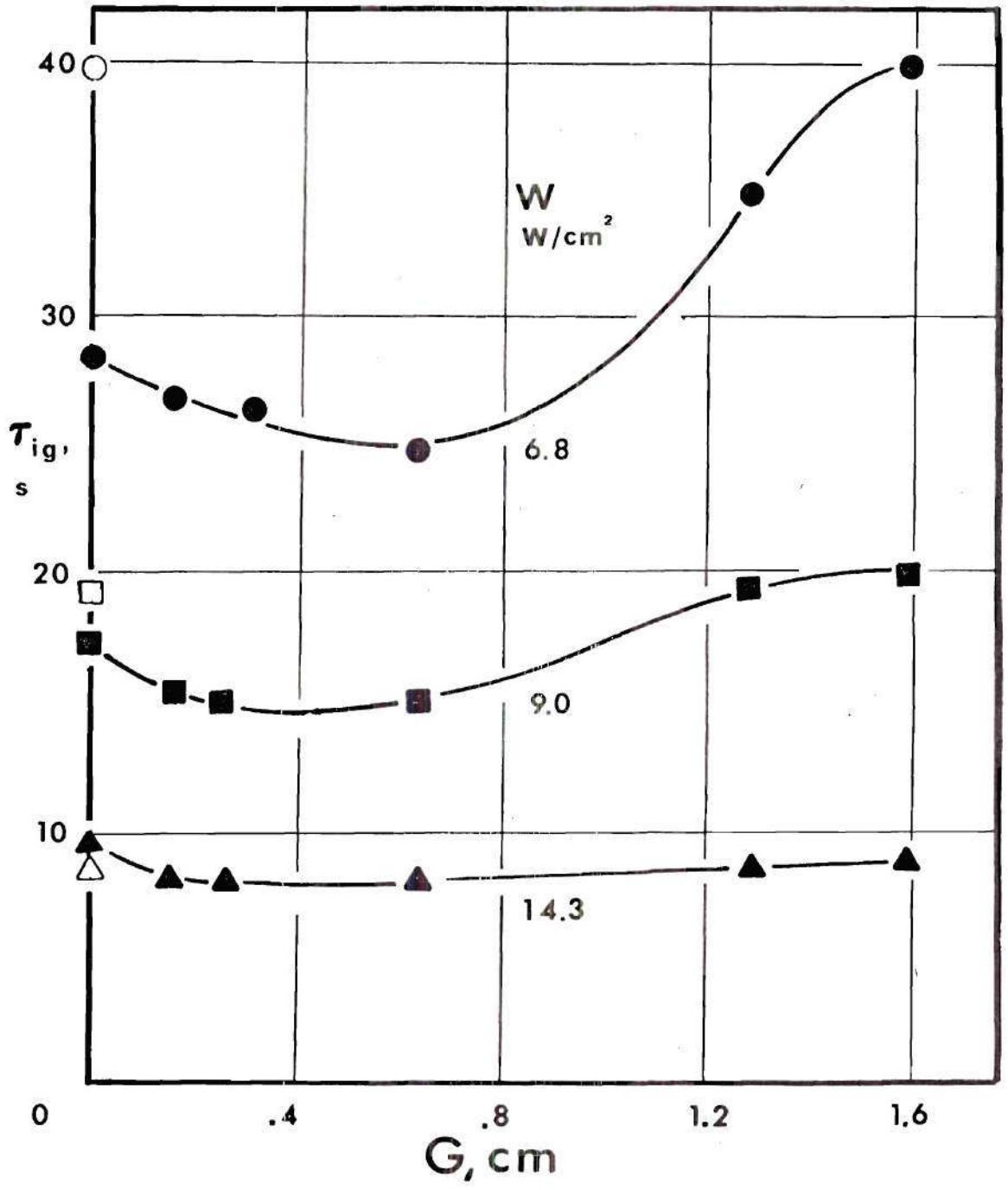

Figure 10. Ignition Time of the Front Fabric as a Function of Spacing (GIRCFF Fabric Number 18 Front and 3 Back; Open Points Denote Single Fabric Ignition Times)

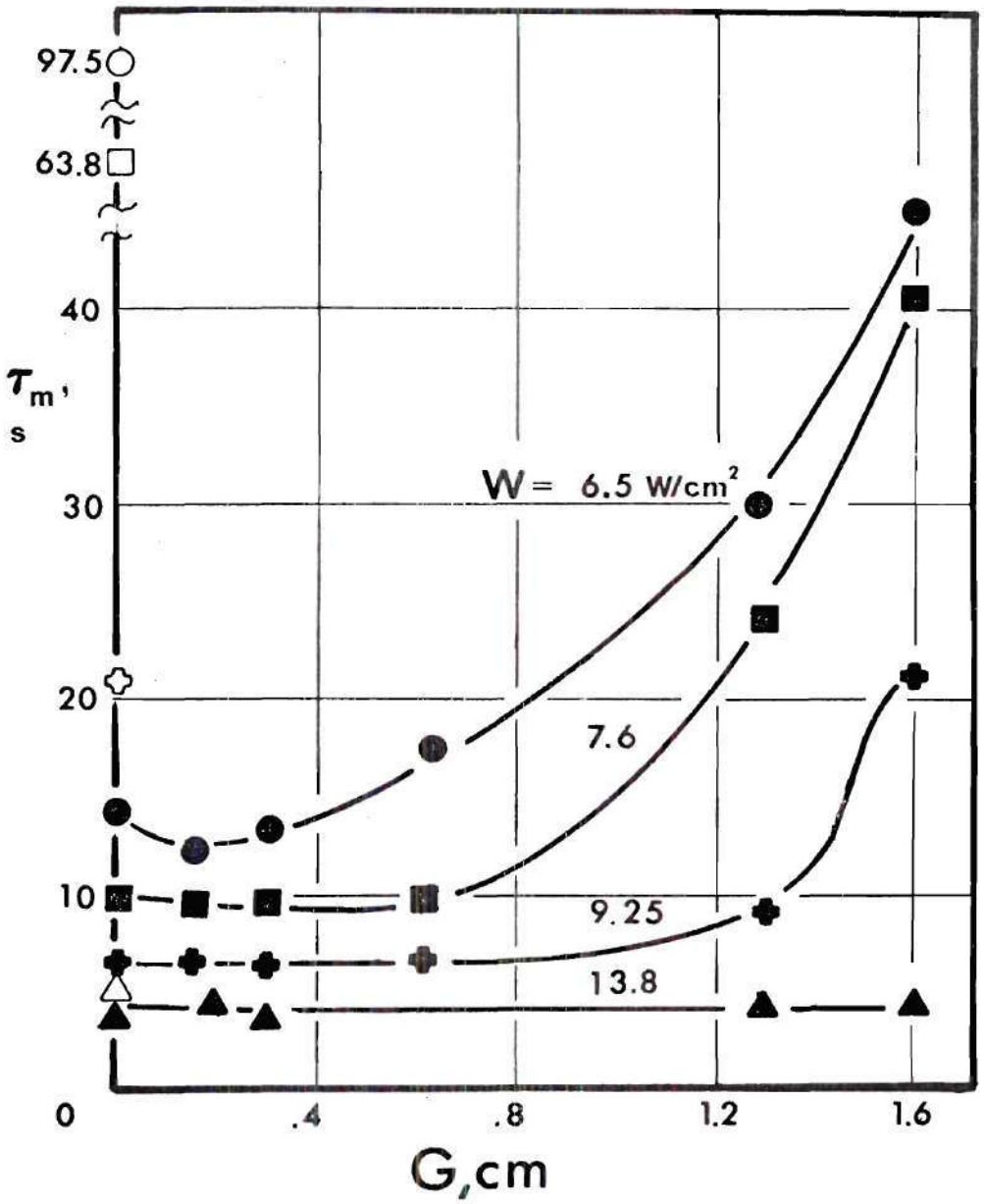

Figure 11. Melting Time of the Fabric as a Function of Spacing (GIRCFF with Fabric Number 2 Front with 5 Back; Open Points Denote Single Fabric Melting Times)

lower than the times for the single fabric, while for an intensity of 14.3 W/cm^2, the trend is reversed. For the front fabric 2 and rear fabric 5 combination, the ignition time for the 0.0 cm gap fabric assembly is lower than the single fabric ignition time for all the fabric intensities.

For the low and medium intensities, the back fabric at 0.0 cm gap acts as a heat sink for the front fabric. The ignition time at this gap is less than the ignition time for a single fabric because heat cannot be conducted away from the front fabric as fast as it can be convected away, which is what happens with a single piece of fabric. For the highest intensities on the fabric number 18 front and fabric number 3 back combinations and fabric number 5 front and 5 back combination, a critical point in the front fabric heat balance is reached where the convection off the rear of the single fabric is not as great as the conduction from the front fabric at 0.0 cm gap.

As shown in Figures 9 through 11, a minimum ignition time for a given heat flux occurs around a gap of .3 to .4 cm. This gap for a minimum ignition time is independent of fabric combination. As the gap is increased from 0.0 cm, the ignition time for a constant heat flux decreases to the minimum point and then increases to the single fabric ignition time. The reason for this behavior can be explained as follows.

At small fabric spacings, the thermal interchange

between the front and rear fabric is due to conduction through the air gap, re-reflectivity and radiative interchange. As the gap increases, the effect of conduction decreases and convection between the two fabrics becomes important. The minimum ignition point is the point where the convection between the two fabrics becomes greater than the conduction. As the gap is further increased, the effect of re-reflectivity diminishes to the point where the front fabric behaves like a single fabric. This occurred at a gap of 1.6 cm.

The effect of the convective heat loss off the back of the front fabric is greater at the lower intensities. As the intensity increases the energy accumulation in the front fabric increases at a faster rate and the effect of convection is less.

From a comparison of the ignition times of fabric number 5 front and fabric number 5 back and fabric number 18 front and 3 back, no differences were noted. There is apparent thermal interaction between fabric layers of the assembly, but there is no evidence of chemical interaction between the fabric layers.

From Table 8 it is seen that painting the inside surfaces of fabric spacers flat black had no effect on ignition time. This shows that the radiant energy reflection from the inside surface of the aluminum spacers is negligible.

CHAPTER IV

ANALYTICAL MODELING OF FABRIC INTERACTION UNDER RADIATIVE HEATING

The objective of the modeling analysis is (i) to predict the ignition time of the front fabric for fabric assemblies under radiative heating and (ii) to apply an ignition criterion incorporating boundary layer ignition to fabric assemblies exposed to radiative heating.

An analytical model is developed to simulate the thermal response of the fabric assembly when the front fabric is suddenly exposed to a uniform and time invariant radiant heat flux. The model is also used to predict the ignition time of the front fabric in the assembly of two fabric layers separated by a specified air gap. For the prediction of fabric ignition times the model also requires an ignition criterion to define the onset of ignition.

4.1. Modeling Analysis

Acree [8] developed an ignition model for a fabric assembly under radiative heating. Ignition was considered to occur when the surface temperature reached the ignition temperature of the fabric. The ignition temperature was obtained using the Setchkin furnace.

Wulff [7,16] developed an ignition model for a single

fabric under radiative heating. His model accounts for the interactions between the solid phase evolving volatiles and surrounding air. Ignition occurs in the gaseous phase as soon as somewhere in the boundary layer a minimum temperature is reached which depends only on the instantaneous local pyrolysate concentration in the pyrolysate mixture.

The analytical model developed in this chapter is a combination of the models of Acree and Wulff. The equations for the front and rear fabrics that were developed by Acree are taken and modified so that they can be used with the boundary layer equations and the ignition criteria used in Wulff's model.

4.2. Problem Formulation

The model considers a two layer, vertical fabric assembly separated by a specified air gap exposed to a time invariant radiative heat flux as shown in Figure 12. The fabric pair is surrounded by semi-infinite, gaseous expanses which represent the system as depicted in Figure 13 at some $\tau > 0$. It is assumed that the vertical dimensions are large with respect to the air gap, the front and rear fabrics are thermally thin, the heat transfer through the fabric layer is one-dimensional and that a negligible fraction of fabric gasified prior to ignition.

For the solid phase the model accounts for

(i) energy storage by both fabrics

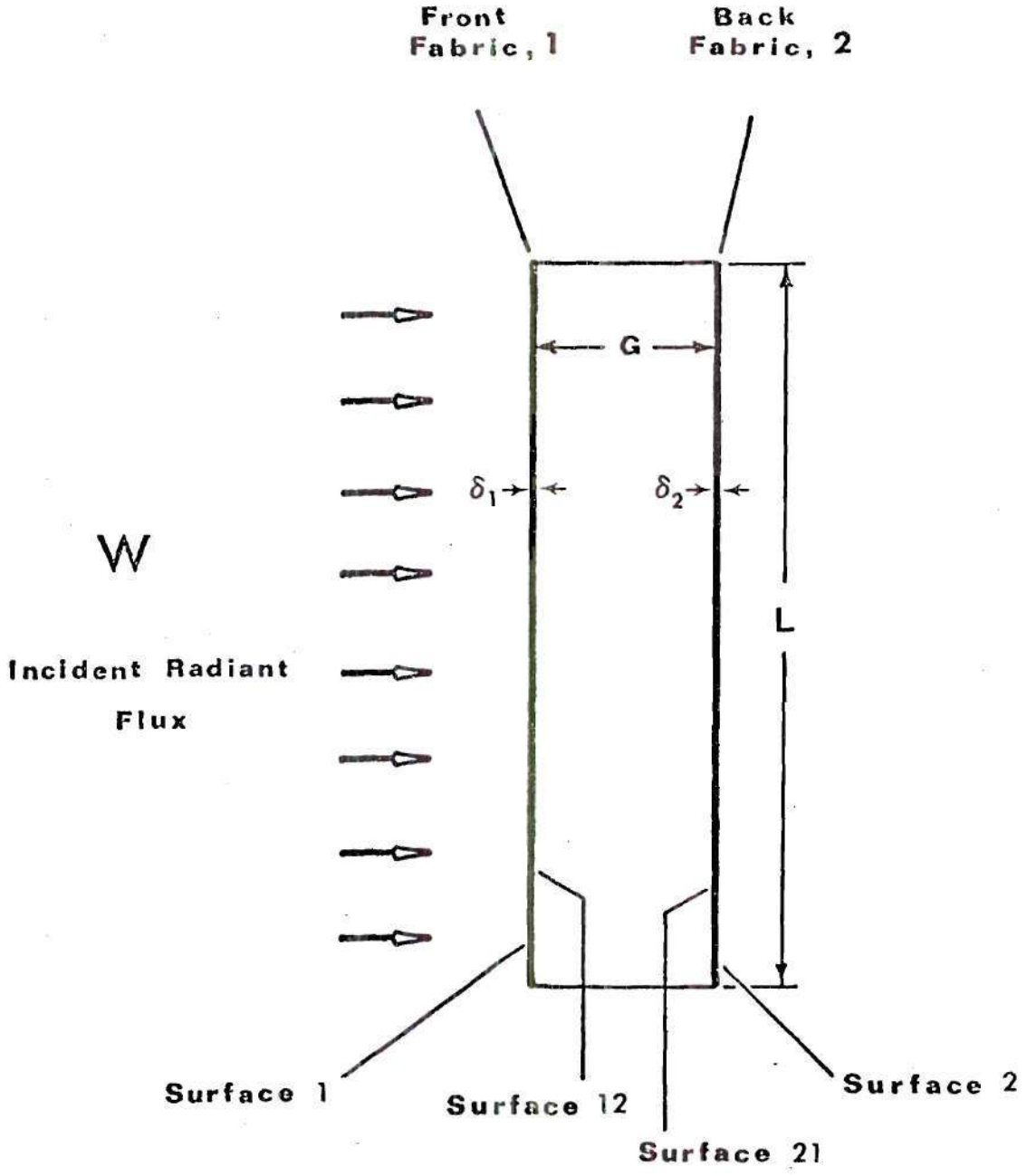

Figure 12. Geometry of the Fabric Assembly

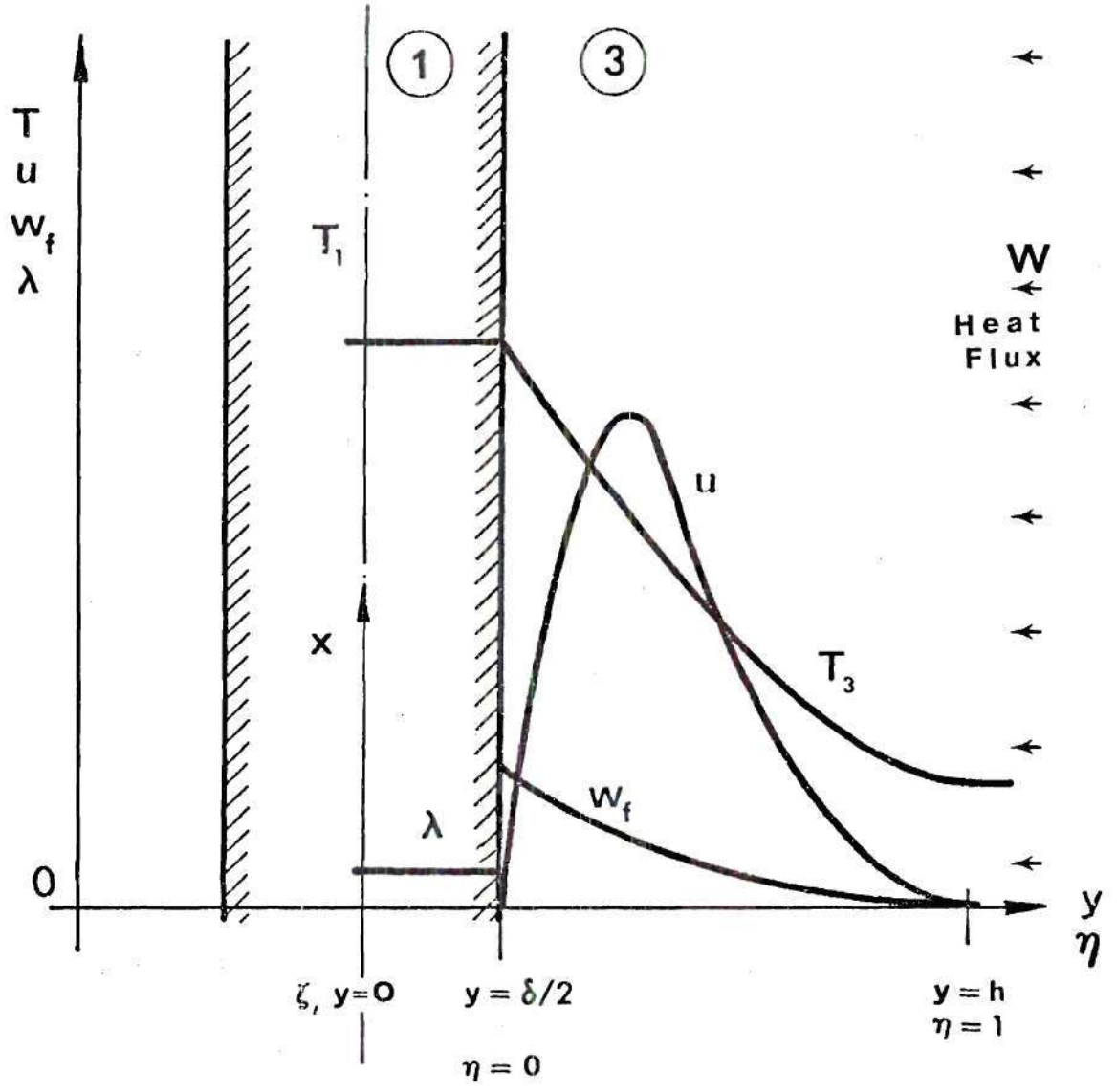

Figure 13. Two-Region System of Front Fabric and Nomenclature

(ii) radiative and convective cooling of surfaces 1 and 2

(iii) radiative interchange between surfaces 12 and 21

(iv) convective interchange between surfaces 12 and 21

(v) temperature dependent fabric properties

(vi) moisture desorption and endothermic gasification of front and rear fabrics

(vii) exothermic combustion of front and rear fabrics (in case of igniting fabrics)

For the gas phase the model assumes constant pressure, negligible reaction in the gas phase prior to ignition, negligible mass injection from solid into boundary layer, negligible injection velocity of pyrolysate and that the molecular weights of air and pyrolysate are equal.

For the gas phase the model accounts for

(i) temperature dependent properties

(ii) temperature, velocity and mass fraction profiles throughout the boundary layer

4.3. Governing Equations

The radiant heating of a fabric assembly accompanied by thermal decomposition and pyrolysate convection is described by the equations of mass, energy and momentum balance. The constitutive laws for conduction, endothermic pyrolysis, moisture desorption, exothermic combustion (for igniting fabrics), and solid and gas phase material

descriptions are needed along with the three balance equations for a solution.

4.3.1. Solid Phase

Two energy conservation equations, one for the front and one for the back fabric, describe the one dimensional heating of the fabric assembly.

The conservation of energy for the front fabric is

$$(\rho\delta)_1 c_1 \frac{dT_1}{d\tau} = \tilde{\alpha}_1^* W - h_1(T_1-T_\infty) - h_{12}(T_1-T_2) - \sigma e_1 F_{1\infty}(T_1^4-T_\infty^4)$$

$$- \sigma F_{12}(T_1^4-T_2^4)/[1/e_1+1/e_2-1] - (\Delta i)_{1,md}\varepsilon_{1,md}(\rho\delta)_{1,o}\frac{d\lambda_{1,md}}{d\tau}$$

$$- (\Delta i)_{1,en}\varepsilon_{1,en}(\rho\delta)_{1,o}\frac{d\lambda_{1,en}}{d\tau} + (\Delta i)_{1,ex}\varepsilon_{1,ex}(\rho\delta)_{1,o}\frac{d\lambda_{1,ex}}{d\tau} \qquad (4.1a)$$

where

$$\tilde{\alpha}_1^* = \tilde{\alpha}_1\left[1 + \frac{\tilde{\tau}_1\tilde{\rho}_2}{1-\tilde{\rho}_1\tilde{\rho}_2}\right] \qquad (4.1b)$$

$\rho\delta$ = specific mass

c = specific heat

T = absolute temperature

τ = time

$\tilde{\alpha}$ = radiative absorptivity

$\tilde{\tau}$ = radiative transmissivity

$\tilde{\rho}$ = radiative reflectivity

W = incident heat flux

h = convective film coefficient

σ = Stephan-Boltzmann constant

e = emissivity

ε = decomposable mass fraction participating in the particular reaction

$F_{1\infty}$ = radiative exchange factor between the front fabric and the atmosphere

F_{12} = radiative exchange factor between the front and back fabric

Δi = reaction enthalpy

λ = fraction of decomposable mass which evolves from fabric

Subscripts 1 and 2 refer to the front and back fabric in the fabric assembly, respectively, and the outside surfaces of the fabrics as defined in Figure 12. Subscripts 12 and 21 refer to the inside surfaces of fabrics 1 and 2, respectively, as shown in Figure 12. Subscripts o, ∞, en, md, en and ex refer to initial conditions, ambient conditions, moisture desorption, endothermic gasification, and exothermic reaction, respectively.

The term on the left side of equation (4.1a) represents the net energy storage of the front fabric. The eight terms on the right side are the total absorbed radiant heat flux,

the convection at surface 1, the convection at surface 12, the radiative cooling of surface 1, the radiative cooling of surface 12, the energy absorbed by moisture desorption in the front fabric, the energy absorbed by endothermic pyrolysis of the front fabric, and the heat liberated by the exothermic reaction of the front fabric. The expression for the absorbed incident radiation includes the effect of the rereflectivity between parallel fabric layers.

The reaction rates of moisture desorption, pyrolysis, and exothermic reaction are described in terms of nth order Arrhenius type relations. The decomposition rates are given by equations of the form

$$\frac{d\lambda}{d\tau} = A(1-\lambda)^n \exp(-E/RT) \tag{4.2}$$

where the reaction kinetic parameters are the pre-exponential factor A, the order of the reaction n, and the activation energy E. R is the universal gas constant. Three such equations each describe the rates of moisture desorption, endothermic pyrolysis, and exothermic reaction.

The pyrolysate mass conservation equation for the front fabric is

$$\partial(\rho_f v_1)/\partial y = r''' \tag{4.3}$$

where r''' is the pyrolysate production rate and v_1 is the Darcy velocity of the evolving pyrolysate.

The equation for conservation of energy for the back fabric is written as

$$(\rho\delta)_2 c_2 \frac{dT_2}{d\tau} = \frac{\tilde{\alpha}_2\tilde{\tau}_1}{1-\tilde{\rho}_1\tilde{\rho}_2} W - h_2(T_2-T_\infty) - h_{21}(T_2-T_1) - \sigma F_{2\infty} e_2 (T_2^4-T_\infty^4)$$

$$-\sigma F_{21}(T_2^4-T_1^4)/[1/e_1 + 1/e_2 - 1] - (\Delta i)_{2,md}\varepsilon_{2,md}(\rho\delta)_{2,o} \frac{d\lambda_{2,md}}{d\tau}$$

$$-(\Delta i)_{2,en}\varepsilon_{2,en}(\rho\delta)_{2,o} \frac{d\lambda_{2,en}}{d\tau} + (\Delta i)_{2,ex}\varepsilon_{2,ex}(\rho\delta)_{2,o} \frac{d\lambda_{2,ex}}{d\tau} \tag{4.4}$$

Three equations of the form of (4.2) are used to describe the decomposition rates of the back fabric by moisture desorption, endothermic gasification, and exothermic reaction.

Expressions for free convection at surfaces 1 and 2 are found from standard heat transfer texts. For the free convection from a flat vertical plate, the heat transfer rate may be represented by [20]

$$(N_{Nu,L}) = 0.59\ (N_{Gr,L}N_{Pr})^{1/4} \tag{4.5}$$

where L is the pertinent scaling length, and the Nusselt, Prandtl, and Grashof numbers are defined by

$$N_{Nu,x} = hL/k \tag{4.6a}$$

$$N_{Pr} = c_p \mu/k \tag{4.6b}$$

$$N_{Gr,L} = g\beta(T_f - T_\infty)L^3/\nu^2 \tag{4.6c}$$

The parameters not yet defined are k, the thermal conductivity, μ, the dynamic viscosity, ν, the kinetic viscosity, g, the acceleration due to gravity, β, the coefficient of thermal expansion, and ν, the kinematic viscosity. Properties are assumed to be those of air and to vary with temperature. The properties for air were obtained from tables in Reference [21].

The problem of the combined effects of conduction and convection in an enclosed air gap (as is the case between surfaces 12 and 21) has been studied by Mull and Peiher [22] and Eckert and Carlson [21]. Previous work has shown that at small air gaps the mode of heat transfer is primarily conduction but as the air gap increases the heat transfer becomes predominantly convective. Jakob [21] has determined that for a Grashof number less than 2000 the heat transfer throughout an air gap is purely conductive while for a Grashof number greater than 2000, the mode of heat transfer is primarily convective. In calculating the Grashof number, the length to be used in equation (4.6) is the fabric separation distance.

If the $N_{Gr,G} < 2000$, the following expression is suggested for the film coefficients for heat transfer through an air medium [21]

$$h_{21} = h_{12} = \frac{k_a}{G} \tag{4.6}$$

where G is the thickness of the air gap. When $N_{Gr,G} > 2000$, the following expression should be used [20]

$$\frac{hL}{k} = 0.18(N_{Gr,G})^{1/4}(\frac{L}{G})^{-1/9} \tag{4.7}$$

where L is the size of the fabric sample.

4.3.2. Gas Phase

The binary mixture of air and pyrolysate in the boundary layer at the heated fabric sample can be described in terms of four state variables T_3, u_3, v_3 and w_f which are governed by four equations, namely the mixture mass conservation

$$\partial\rho_3/\partial\tau + \partial(\rho u)_3/\partial x + \partial(\rho v)_3/\partial y = 0 \tag{4.8}$$

the pyrolysate mass conservation

$$\rho_3 \frac{\partial w_f}{\partial \tau} + (\rho u)_3 \frac{\partial w_f}{\partial x} + (\rho v)_3 \frac{\partial w_f}{\partial y} = \frac{\partial}{\partial y}\left[\rho_3 D \frac{\partial w_f}{\partial y}\right] \tag{4.9}$$

the momentum balance in the x-direction

$$\rho_3 \frac{\partial u_3}{\partial \tau} + (\rho u)_3 \frac{\partial u_3}{\partial x} + (\rho v)_3 \frac{\partial u_3}{\partial y} = g(\rho_\infty - \rho_3) + \frac{\partial}{\partial y}\left[\mu \frac{\partial u_3}{\partial y}\right] \qquad (4.10)$$

and the conservation of energy

$$\rho_3 \frac{\partial i_3}{\partial \tau} + (\rho u)_3 \frac{\partial i_3}{\partial x} + (\rho v)_3 \frac{\partial i_3}{\partial y} = \frac{\partial}{\partial y}\left[k_3 \frac{\partial T_3}{\partial y} + (i_f - i_a)\rho_3 D \frac{\partial w_f}{\partial y}\right]$$

$$+ \mu\left[\frac{\partial u_3}{\partial y}\right]^2 \qquad (4.11)$$

Here the subscripts 3, f, and a designate, respectively, gaseous region (3), pyrolysate species and air. Symbols ρ, T, u, v represent density, temperature, vertical and horizontal velocity components. D and $w_f = \rho_f/\rho_3$ stand for diffusion coefficient and mass fraction, respectively.

The four conservation equations (4.8) through (4.11) must be supplemented by constitutive descriptions for wall shear stress, heat and mass transport, thermal and caloric mixture behavior.

The thermal equation of state is

$$\rho_3 = p/(RT_3) \qquad (4.12)$$

and the caloric equation of state calculates

$$i_3 = \overline{c_{p,3}}\ (T_3 - T_\infty) \tag{4.13}$$

the excess enthalpy of the mixture at the environmental temperature T_∞.

Equations describing wall shear and heat transfer at the solid surfaces are necessary in anticipation of recasting equations (4.8) through (4.11) in integral form. The local shear stress is approximated by [7,16]

$$s = .332\rho_3 u_m^2 (N_{Re})_x^{-1/2}, \text{ for } N_{Re,x} \leq 5(10^5) \tag{4.14}$$

or

$$s = 0.0225\rho_3 u_m^2 (\nu_3/u_m h(x)^{-1/4}, \text{ for } N_{Re,x} > 5.5(10^5) \tag{4.15}$$

while the convective heat flux at the surface, averaged over the heated length L, is computed for laminar flow from [7,15]

$$q_y'' = 0.508\ k_3 T_\infty [g[T_1 - T_\infty]/T_\infty \nu^2 L]^{1/4}$$

$$\text{for } N_{Re,x} < 5.0(10^5) \tag{4.16}$$

For turbulent flow, the convective flux is given by [7,15]

$$q''_y = 0.0225\ \rho_3 c_{p,3} u_m (T_{3,\delta} - T_\infty) \left(\frac{\nu_3}{u_m h(x)}\right)^{1/4} N_{Pr}^{-2/3}$$

$$\text{for } N_{Re,x} > 5.5(10^5) \qquad (4.17)$$

where u_m represents the local maximum upward velocity.

Equations (4.14) through (4.17) are correct only in the limit of vanishing pyrolysate evolution. The approximation is valid except for cases of very low heating intensities [7].

4.3.3. Initial and Boundary Conditions

$\tau \leq 0$

$$T_1 = T_2 = T_3 = T_o = T_\infty \qquad \text{for all } (x,y) \qquad (4.18a)$$

$$\lambda_{en} = \lambda_{ex} = \lambda_{md} = 0 \qquad \text{for } -\infty<x<\infty,\ -\delta/2 \leq y \leq \delta/2 \qquad (4.18b)$$

$$u = v = 0 \qquad \text{for all } (x,y) \qquad (4.18c)$$

$\tau > 0$

$$\left.\begin{aligned} & v_1 = 0,\ \partial T_1/\partial y = 0 \text{ at } y = 0 \\ & (\rho v)_1 = (\rho v)_3 \\ & u_3 = 0 \\ & T_1 = T_3 \\ & (q''_y)_1 = (q''_y)_3 \\ & q''_{r,y}(\delta/2) = (1-\tilde{\rho})W \end{aligned}\right\} \quad -\infty<x<\infty,\ y = \delta/2 \qquad (4.19a)$$

$$\left.\begin{aligned} u_3 &= 0 \\ T_3 &= T_\infty \\ q''_y &= 0 \\ w_f &= 0 \end{aligned}\right\} \quad -\infty<x<\infty,\ y \geq \delta/2 + h(x) \qquad (4.19b)$$

4.4. Solution

An integral analysis is used to transform the local conservation equations (4.8) through (4.11), through spatial integration, into global description which retains all essential features of the preignition processes. The six balance equations, equations (4.1), (4.4) and (4.8) through (4.11), define six system state variables which are considered to be a part of the components Y_1, Y_2, ... Y_{11} of the eleven dimensional vector $\underset{\sim}{Y}$. Chosen as the components are:

the nondimensional front fabric temperature

$$Y_1 = T_1/T_\infty - 1 \qquad (4.20)$$

the degree of decomposition for the front fabric

$$Y_2 = \lambda_{en,1} \qquad (4.21)$$

the Reynolds number

$$Y_3 = UH/\nu_3 \tag{4.22}$$

the nondimensional maximal boundary layer thickness

$$Y_4 = H/L \tag{4.23}$$

the pyrolysate mass fraction at the surface

$$Y_5 = w_{f,\delta} \tag{4.24}$$

the nondimensional back fabric temperature

$$Y_6 = T_2/T_\infty - 1 \tag{4.25}$$

the degree of moisture desorption for the front fabric

$$Y_7 = \lambda_{md,1} \tag{4.26}$$

the degree of exothermic combustion for the front fabric

$$Y_8 = \lambda_{ex,1} \tag{4.27}$$

the degree of moisture desorption for the back fabric

$$Y_9 = \lambda_{md,2} \tag{4.28}$$

the degree of pyrolysis gasification for the back fabric

$$Y_{10} = \lambda_{en,2} \tag{4.29}$$

and the degree of exothermic combustion for the back fabric

$$Y_{11} = \lambda_{ex,2} \tag{4.30}$$

where $U = u_m(L)$ and $H = h_m(L)$, with L representing the height of the heated surface.

These state variables will be shown to suffice for the description of the two-region system at any time τ and for the prediction of ignition time τ_{ig}.

Similarity is assumed throughout the boundary layer ($N_{Pr} = N_{Sc} = 1$) except initially and near the leading edge. Similarity provides an approximate relationship between the temperature, velocity and mass fraction profiles.

The normalized independent variables are introduced for

time

$$\tau^* = \tilde{\alpha}_1^* W/[(\rho\bar{c})_1 \delta T_\infty] = \tau/\tau_{ref} \tag{4.31}$$

vertical coordinate

$$\xi = x/L, \qquad 0 \leq \xi \leq 1 \tag{4.32}$$

and lateral coordinates

$$\eta = \frac{(y-\frac{\delta}{2})}{h(x)}, \qquad 0 \leq \eta \leq 1 \tag{4.33}$$

in the gaseous phase.

4.4.1. Integral Balance Equations

The energy equations (4.1) and (4.4) for the front and rear fabric are already ordinary differential equations. The model that was used for the front and rear fabrics is a form of the integral analysis where the temperature profile is a constant value. The constant temperature profile throughout the fabric arises from the assumption that the fabrics are thermally thin, that the fabric thickness is so small that no temperature gradient exists throughout the fabric.

The pyrolysate mass conservation equation (4.3) is integrated between 0 and $\delta/2$

$$(\rho v)_1 = (\Delta\rho)_1 \int_0^{\delta/2} \dot{\lambda}_{en,1}\, dy \tag{4.34}$$

The local conservation equations (4.8) through (4.11) will be spatially integrated to obtain ordinary differential equations. Before carrying out the integration, the mass flux $(\rho v)_3$ is eliminated from the momentum balance, equation (4.10) and from the energy balance, equation (4.11), with the

aid of the mass conservation equation (4.8) [16].

The lateral similarity profiles for the gaseous boundary layer are

$$\psi_1(\eta,\underset{\sim}{Y}) = T_3(x,y,\tau)/T_\infty - 1 \tag{4.35}$$

$$\psi_2(\eta,\underset{\sim}{Y}) = u_3(x,y,\tau)/u_m(x) - 1 \tag{4.36}$$

$$\psi_3(\eta,\underset{\sim}{Y}) = w_f(x,y,\tau)/Y_5 \tag{4.37}$$

where ψ_1, ψ_2 and ψ_3 are the profiles for temperature, velocity and pyrolysate mass fraction throughout the boundary layer, respectively. The vertical variations of momentum and energy boundary layer thickness are approximated with

$$h(x)/H = \xi^{\bar{n}} \tag{4.38}$$

and the maximum velocity in every profile is approximated with

$$u_m(x)/U = \xi^{\bar{m}} \tag{4.39}$$

where

$$\left.\begin{aligned} \bar{m} &= 1/2 \\ \bar{n} &= 1/2 \text{ for } N_{Re,L} \leq 5.5(10^5) \\ \bar{n} &= 7/10 \text{ for } N_{Re,L} \geq 5.5(10^5) \end{aligned}\right\} \tag{4.40}$$

The three functions ψ_i are conveniently expressed by power polynomials with $\underset{\sim}{Y}$-dependent coefficients $b_{ij}(\underset{\sim}{Y})$

$$\psi_i = \sum_{j=0}^{M_i} b_{ij}\eta^j, \qquad i = 1,2,3 \tag{4.41}$$

The coefficients are chosen such that equations (4.41) must satisfy equations (4.18) and (4.19).

A parabolic mixture temperature profile implies [7]

$$b_{10} = Y_1,\ b_{11} = -2Y_1,\ b_{12} = Y_1 \tag{4.42}$$

The velocity profile was chosen to be represented by [7]

$$b_{20} = 0,\ b_{22} = -2b_{21},\ b_{23} = -b_{21}$$

and

$$b_{21} = \frac{1+m+n}{\pi_6}\ \frac{Y_4^2}{Y_3} \tag{4.43}$$

where π_6 is defined in Table 3.

Substitution of the three lateral profiles, equations (4.35), (4.36), (4.37) into the three balance equations (4.9), (4.10) and (4.11) yields at first, after integration over η from $\eta = 0$ to $\eta = 1$, three partial differential equations in ξ and τ^*. The final average process is carried out by integrating from $\xi = 0$ to $\xi = 1$. The integrations

Table 3. Scaling Groups for Boundary Layer Equations [16]

$$\pi_1 = T_o/T_\infty - 1$$

$$\pi_2 = (\Delta\rho/\rho)_1$$

$$\pi_3 = \bar{c}_{p,1}/\bar{c}_1$$

$$\pi_4 = \pi_2 \Delta i_1/(\bar{c}_1 T_\infty)$$

$$\pi_5 = gL\tau_{ref}/\nu_3$$

$$\pi_6 = \nu_3 \tau_{ref}/L^2$$

$$\pi_7 = \bar{c}_{p,1}/\bar{c}_{p,3}$$

$$\pi_8 = (\delta/2)(\Delta\rho)_1/(L\rho_\infty)$$

$$\pi_9 = \nu_3^3 \tau_{ref}/(L^4 c_{p,3} T_\infty)$$

$$\pi_{10} = N_{Sc}$$

$$\pi_{11} = N_{Pr}$$

over ξ yield

$$-P_{22}Y_3\dot{Y}_1+P_{21}\dot{Y}_3 = (1+\bar{m}+\bar{n})\left[\frac{\pi_5 P_{24}Y_4}{1+\bar{n}} - \frac{\pi_6 P_{23}Y_3^2}{Y_4} - s^*\right] \quad (4.44)$$

$$P_{32}/(1+\bar{n})Y_4\dot{Y}_1-\pi_7\pi_8\left(\sum_{j=0}^{2} Q_{ij}P_{ij}\right)Y_1\dot{Y}_2+P_{31}/(1+\bar{n})\dot{Y}_4 =$$

$$\frac{\pi_7\pi_8}{\pi_2\pi_3}\,q^* + \frac{\pi_9 P_{34}}{1+2\bar{m}-\bar{n}}\,\frac{Y_3^2}{Y_4^3} - \pi_6\left[P_{33}Y_3 + \frac{(1-\pi_7)P_{44}}{\pi_{10}(1+\bar{m}+\bar{n})}\,\frac{Y_1Y_5}{Y_4(1+Y_1)}\right] \quad (4.45)$$

and

$$-P_{42}Y_4Y_5/(1+\bar{n})\dot{Y}_1-\pi_8\left(\sum_{j=0}^{2} Q_{ij}P_{ij}\right)\dot{Y}_2+P_{41}/(1+\bar{n})Y_5\dot{Y}_4+P_{41}/(1+\bar{n})Y_4\dot{Y}_5$$

$$= -\pi_6\{P_{44}Y_5/[\pi_{10}Y_4(1-\bar{n})]+P_{43}Y_3Y_5\} \quad (4.46)$$

The scaling parameters π_1 through π_{11} are defined in Table 3 and the profile integrals P_{ij} are evaluated in closed form for equations (4.35) through (4.36) and are listed in Table 4.

The coefficients $Q_{ij}(\underset{\sim}{Y})$ stand for

$$Q_{10} = 1-Y_1Q_{11} \quad (4.47a)$$

$$Q_{11} = 1/(1+Y_1)^2 \quad (4.47b)$$

Table 4. Profile Integrals P_{ij} [16]

$P_{10} = 1$

$P_{11} = Y_1 + q^*/3$

$P_{12} = \sum_{j=0}^{3} a_{2j}/(j+1)$, $a_{23} = 1 - \sum_{j=0}^{2} a_{2j}$, see note 1 below

$P_{13} = [5Y_1(3Y_1+2q^*)+2(q^*)^2]/15$

$P_{14} = P_{12}Y_1$

$P_{21} = b_{21}[1/2(1+Z_1)-Z_2]^{**}$, $Z_1 = (1/Y_1)\ln(1+Y_1)$

$Z_2 = (1/Y_1{}^{1/2})\tan^{-1}Y_1{}^{1/2}$

$P_{22} = b_{21}(1+2Z_1-3Z_2)/(2Y_1{}^2)$

$P_{23} = b_{21}[(Y_1^2-10Y_1+30)/30 - (1-Y_1)Z_2 - Y_1Z_1]Y_1^{-3}$

$P_{24} = 1-Z_2$

$P_{25} = Z_2$

$P_{31} = P_{24}$

$P_{32} = [Z_2 - 1/(1+Y_1)]/(2Y_1)$

$P_{33} = b_{21}[Y_1+6(2Z_2-Z_1-1)]/(12Y_1)$

$P_{34} = 2b_{21}^2/15$

$P_{41} = (1-Z_2)/Y_1$

$P_{42} = (Z_2+Y_1/3-1)Y_1^2$

$P_{43} = P_{33}/Y_1$

$P_{44} = -2$

Note that all integrals remain finite as $\underset{\sim}{Y} \to \underset{\sim}{0}$

$^{**}b_{21} = (1/\pi_6)(1+\bar{m}-\bar{n})(Y_4^2/Y_3)s^*$

Note 1. $P_{12} = 0$ for thermally thin materials.

$$Q_{12} = -nY_2/(1-Y_2) \tag{4.47c}$$

The first and second terms on the left hand side of equation (4.44) represents the rates of momentum decay and growth, respectively, due to density reduction resulting from the heating process, and due to vertical upward acceleration. The first term on the right-hand side stands for the driving buoyancy, the second term for the momentum flux at the top of the heated section, and the last term is the average retarding shear at the solid surface.

$$s^* = (\tau_{ref}/\mu)\int_0^1 s(\xi)d\xi \tag{4.48}$$

The first, second and third terms on the left-hand side of equation (4.45) are the contributions to the total enthalpy rise, resulting from temperature rise, pyrolysate injection and boundary layer growth, respectively. On the right-hand side of equation (4.45) stand in this order, conduction from the hot solid to the boundary layer, viscous dissipation, enthalpy flux leaving at the top of the heated section and pyrolysate diffusion due to the concentration gradient. The pyrolysate balance, equation (4.46), consists of the left-hand side of the terms representing the rate of pyrolysate accumulation due to the rise in mixture density, injection, boundary layer growth and increasing pyrolysate concentration, in that order. On the right hand side of equation (4.46) is

simply the supply of pyrolysate because of molecular diffusion from the solid into the boundary layer, less the convective loss at the top of the heated section (notice from Table 4.2 that $P_{44} < 0$).

The energy equations for the front and rear fabrics, equations (4.1) and (4.4), respectively, and six equations of the form of equation (4.2) for moisture desorption, endothermic pyrolysis, and exothermic reaction for the front and back fabric were normalized using the relevant scaling parameters for time, equation (4.31), and the degree of fabric decomposition, equations (4.21) and equations (4.26) through (4.30).

The above substitutions yield the following normalized differential energy equations for the front fabric. The

$$\frac{dY_1}{d\tau^*} = \pi_{100} - \pi_{101} Y_1 - \pi_{102}(Y_1 - Y_6) - \pi_{103}[(Y_1+1)^4 - 1]$$

$$- \pi_{104}[(Y_1+1)^4 - (Y_6+1)^4] - \pi_{104}[(Y_1+1)^4 - (Y_9+1)^4] - \pi_{105} \frac{dY_7}{d\tau^*}$$

$$- \pi_{106} \frac{dY_7}{d\tau^*} + \pi_{107} \frac{dY_8}{d\tau^*} \qquad (4.49)$$

decomposition rates for the solid are given in terms of these nth-order Arrhenius type relations.

$$\frac{dY_7}{d\tau^*} = \pi_{108}(1-Y_7)^{\pi_{114}}\exp(\pi_{111}/(Y_1+1)) \qquad (4.50)$$

$$\frac{dY_2}{d\tau^*} = \pi_{109}(1-Y_2)^{\pi_{115}}\exp(\pi_{112}/(Y_1+1)) \qquad (4.51)$$

$$\frac{dY_8}{d\tau^*} = \pi_{110}(1-Y_8)^{\pi_{116}}\exp(\pi_{113}/(Y_1+1)) \qquad (4.52)$$

The normalized energy conservation equation for the back fabric is

$$\frac{dY_6}{d\tau^*} = \pi_{200}-\pi_{201}Y_6-\pi_{202}(Y_6-Y_1)-\pi_{203}((Y_6+1)^4-1)$$

$$-\pi_{204}[(Y_6+1)^4-(Y_1+1)^4]-\pi_{205}\frac{dY_9}{d\tau^*}-\pi_{206}\frac{dY_{10}}{d\tau^*}+\pi_{207}\frac{dY_{11}}{d\tau^*}$$

The decomposition rates for the rear fabric are expressed by three normalized equations

$$\frac{dY_9}{d\tau^*} = \pi_{208}(1-Y_9)^{\pi_{214}}\exp(\pi_{211}/(Y_6+1)) \qquad (4.53)$$

$$\frac{dY_{10}}{d\tau^*} = \pi_{209}(1-Y_{10})^{\pi_{215}}\exp(\pi_{212}/(Y_6+1)) \qquad (4.54)$$

$$\frac{dY_{11}}{d\tau^*} = \pi_{210}(1-Y_{11})^{\pi_{216}}\exp(\pi_{213}/(Y_6+1)) \qquad (4.55)$$

The 34 scaling groups for the set of eight equations (4.49) through (4.55) are defined in Tables 5 and 6.

4.4.2. Numerical Integration

Equations (4.44) through (4.46) and (4.49) through (4.55) are of the form

$$\sum_{j=1}^{11} C_{ij}(Y_1,\ldots,Y_{11};\tau^*;\pi_1,\ldots,\pi_{14};\pi_{100},\ldots,\pi_{116};\pi_{200},\ldots\pi_{216})\dot{Y}_j =$$

$$B_i(Y_1,\ldots,Y_{11};\tau^*;\pi_1,\ldots,\pi_{14};\pi_{100},\ldots,\pi_{116};\pi_{200},\ldots,\pi_{216}),$$

$$i = 1,\ldots,11 \qquad (4.56)$$

The coefficient matrix is invertible for non-zero boundary layer thickness $Y_4 > 0$. Where

$$\dot{Y}_j = \sum_{j=1}^{11} C_{ij}^{-1}B_i, \quad j = 1,11 \qquad (4.57)$$

since $\underset{\sim}{B}$ is bounded for $Y_4 > 0$ [7].

The initial conditions require

$$\underset{\sim}{Y}(0) = \{\pi_1,0,0,0,0,\pi_1,0,0,0,0,0\} \qquad (4.58)$$

Equation (4.57) was integrated subject to a fourth-order Runge-Kutta algorithm with automatic time step ($\Delta\tau^*$) selection, controlled by specifying the admissible relative and absolute errors per time step.

Table 5. Scaling Groups for the Front Fabric

$\pi_{100} = 1$

$\pi_{101} = h_1 T_\infty / W\tilde{\alpha}_1^*$

$\pi_{102} = h_{12} T_\infty / W\tilde{\alpha}_1^*$

$\pi_{103} = \sigma e_1 F_{1\infty} T_\infty^4 / W\tilde{\alpha}_1^*$

$\pi_{104} = \sigma F_{12} T_\infty^4 / W\tilde{\alpha}_1^* [1/e_1 + 1/e_2 - 1]$

$\pi_{105} = (\Delta i)_{md,1} \varepsilon_{md,1} / c_1 T_\infty$

$\pi_{106} = (\Delta i)_{en,1} \varepsilon_{en,1} / c_1 T_\infty$

$\pi_{107} = (\Delta i)_{ex,1} \varepsilon_{ex,1} / c_1 T_\infty$

$\pi_{108} = t_{ref} A_{md,1}$

$\pi_{109} = t_{ref} A_{en,1}$

$\pi_{110} = t_{ref} A_{ex,1}$

$\pi_{111} = -E_{md,1} / RT_\infty$

$\pi_{112} = -E_{en,1} / RT_\infty$

$\pi_{113} = -E_{ex,1} / RT_\infty$

$\pi_{114} = n_{md,1}$

$\pi_{115} = n_{en,1}$

$\pi_{116} = n_{ex,1}$

Table 6. Scaling Groups for the Back Fabric

$$\pi_{200} = t_{ref}[\tilde{\tau}_1\tilde{\alpha}_2/(1-\tilde{\rho}_1\tilde{\rho}_2)]W/(\delta\rho)_2 c_2 T_\infty$$

$$\pi_{201} = t_{ref} h_2/(\rho\delta)_2 c_2$$

$$\pi_{202} = t_{ref} h_{21}/(\rho\delta)_2 c_2$$

$$\pi_{203} = t_{ref}\sigma e_2 F_{2\infty} T_\infty^3$$

$$\pi_{204} = t_{ref}\sigma F_{21} T_\infty^3/(1/e_1 + 1/e_2 - 1)(\rho\delta_2)(c_2)$$

$$\pi_{205} = (\Delta i)_{md,2\ md,2}/T_\infty c_2$$

$$\pi_{206} = (\Delta i)_{en,2}\varepsilon_{en,2}/T_\infty c_2$$

$$\pi_{207} = (\Delta i)_{ex,2}\varepsilon_{ex,2}/T_\infty c_2$$

$$\pi_{208} = t_{ref} A_{md,2}$$

$$\pi_{209} = t_{ref} A_{en,2}$$

$$\pi_{210} = t_{ref} A_{ex,2}$$

$$\pi_{211} = -E_{md,2}/RT_\infty$$

$$\pi_{212} = -E_{en,2}/RT_\infty$$

$$\pi_{213} = -E_{ex,2}/RT_\infty$$

$$\pi_{214} = n_{md,2}$$

$$\pi_{215} = n_{en,2}$$

$$\pi_{216} = n_{ex,2}$$

Having predicted the surface temperature $Y_1(\tau^*)$, the pyrolysate concentration $Y_5(\tau^*)$ at the surface, and the time rate of pyrolysate evolution $\dot{Y}_2 \sum_{j=0}^{2} P_{ij}Q_{ij}$, the ignition criterion can be applied [16] for the prediction of ignition time of the front fabric in the assembly.

4.5. Ignition Criterion

To apply the ignition criterion, certain assumptions are necessary.

(1) There exists, for every pyrolysate concentration $w_{f1} \leq w_f \leq w_{fu}$ in air between the lower and upper concentration limits w_{f1} and w_{fu}, respectively ($0 < w_{f1} < w_{fu} < 1$) a minimum temperature $T_{ig}(w_f)$ at which spontaneous ignition occurs.

(2) A concentration profile $w_f(x,y,\tau)$ establishes itself during pyrolysate evolution from the heated surface which, after substitution into the experimentally defined function $T_{ig}(w_f)$, defines for sufficiently large values of time τ a necessary minimum temperature distribution $T_{ig}(x,y,\tau)$.

(3) The actual mixture temperature $T_3(x,y,\tau)$ approaches $T_{ig}(x,y,\tau)$ from below, starting from $T_3 = T_o$, until at the instant τ_{ig} at some point (x,y), $T_3(x,y,\tau_{ig}) = T_{ig}(x,y,\tau_{ig})$ for the first time.

The concentration dependent minimum ignition temperature

$$T_{ig} = f(w_f), \qquad 0 < w_f < 1 \tag{4.59}$$

is necessary to apply the ignition criterion. The function $f(w_f)$ is experimentally determined and varies for different fabric compositions. Figures 14 and 15 show the $T_{ig}(w_f)$ curves for fabric number 4, a cotton, and for fabric number 2, a polyester, respectively. The pyrolysate ignition temperatures as a function of pyrolysate concentration have been measured using the Lower Ignition Temperature and Concentration Apparatus (LITACA). Description of this apparatus and procedure used have been detailed in References [7,17].

The equation for the $T_{ig}(w_f)$ curve of pyrolysate gases from fabric number 4 was used in the analysis for fabrics number 5 and 18 since they are all 100% cotton fabrics.

The air surrounding an irradiated solid is heated indirectly by that solid, such that the initially low air temperature rises most rapidly at the heated surface. From the concave shape of the curve representing $T_{ig}(w_f)$ as seen in Figures 14 and 15, it is seen that at low mass fractions, high temperatures are required for ignition. As w_f increases, T_{ig} decreases until a minimum T_{ig} is reached. If w_f still increases, higher T_{ig} are needed for ignition. This indicates that ignition by radiative heating occurs when the surface temperature Y_1 reaches a minimum value.

Substitution of equation (4.32) into equation (4.59) yields

$$\psi_1(Y_{1,\eta}) = T_{ig}/T_\infty - 1 = \psi_{ig}(Y_{5,\eta}) \qquad (4.60)$$

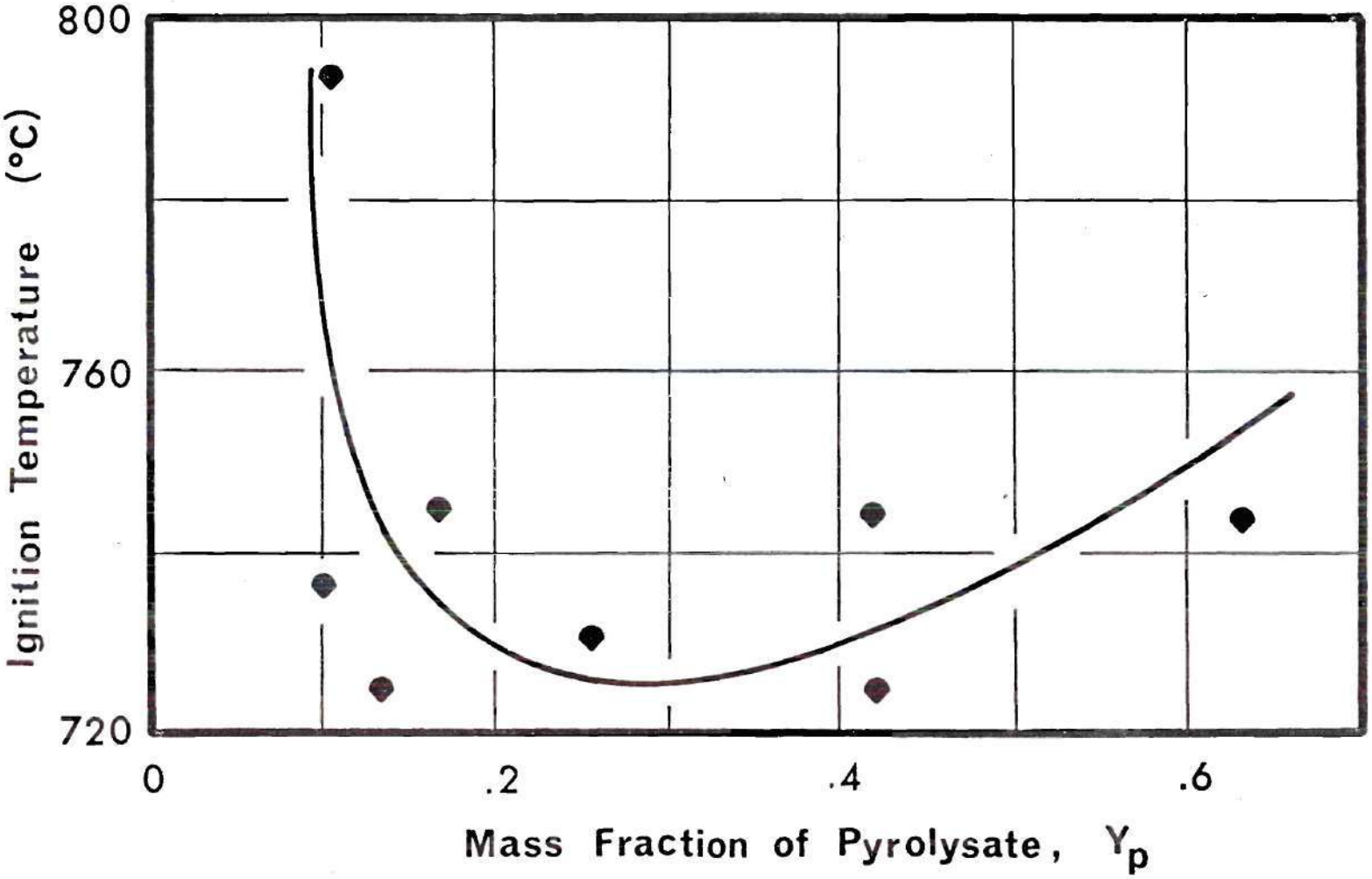

Figure 14. Minimum Ignition Temperatures of Pyrolysate-Air Mixture (Pyrolysate gases generated from fabric number 4) [17]

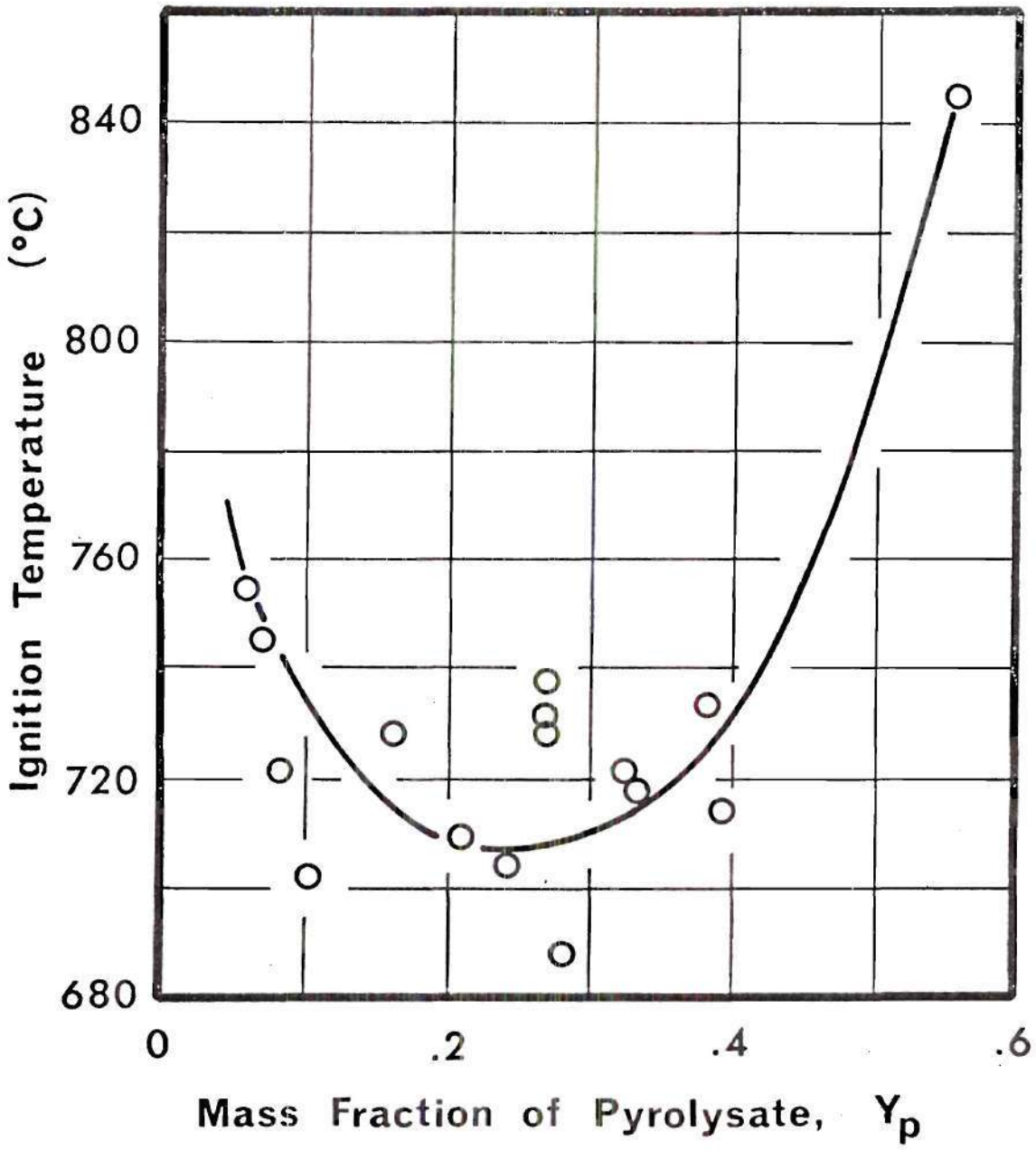

Figure 15. Minimum Ignition Temperature of Pyrolysate-Air Mixture (Pyrolysate gases generated from GIRCFF fabric number 2) [23]

Ignition occurs at $\tau^* = \tau^*_{ig}$ and $\eta = \eta_{ig}$ when and where

$$\psi_1(Y_1, \eta) = \psi_{ig}(Y_5, \eta) \tag{4.61}$$

for the first time. As long as $\tau^* \leq \tau^*_{ig}$, ignition occurs at the surface, $\eta = 0$, if for the instantaneous value of $Y_5(\tau^*)$

$$\frac{\partial \psi_{ig}}{\partial \eta} \geq \frac{\partial \psi_1}{\partial \eta} \quad \text{at } \eta = 0 \tag{4.62}$$

as soon as

$$Y_1 = Y_{ig} = \psi_{ig}(Y_{5,0}) \tag{4.63}$$

which defines the minimum surface temperature in terms of the current fuel concentration. The critical surface temperature Y_{ig} is reached while there is still sufficient oxygen at the surface. If the pyrolysate concentration reaches saturation, $Y_5 = 1$, before the surface temperature reaches sufficiently high values then ignition occurs at the distance $\eta = \eta_{ig}$ from the surface and as soon as [7]

$$\begin{aligned} \Lambda_1(Y_{ig}, Y_5, \eta_{ig}) &= \psi_{ig} - Y_1 = 0 \\ \Lambda_2(Y_{ig}, Y_5, \eta_{ig}) &= \partial/\partial\eta \; \Lambda_1 = 0 \end{aligned} \tag{4.64}$$

Elimination of η_{ig} yields the ignition criterion in terms of the instantaneous pyrolysate concentration at the surface.

$$Y_1 = Y_{ig} = Y_{ig}(Y_5) \tag{4.65}$$

The system of equations (4.64) can be solved during integration of equations (4.57) and equation (4.58). A Newton-Raphson iteration scheme serves to terminate integration when equation (4.65) is satisfied. This yields the required time τ^*_{ig} of ignition.

4.6. Results

Ignition time predictions for the front fabric were obtained for two igniting and one melting fabric assembly. Both heating intensity and inter-layer spacing were varied, and the predicted and experimental destruction times are shown in Tables 7, 8 and 9 for fabric combinations number 5 front and 5 back, number 18 front and 3 back, and number 2 front and 5 back, respectively.

The predicted ignition times shown in Tables 7, 8 and 9 were obtained from the solution of the model discussed in the previous section. To predict an ignition time, an input of 63 variables was required, many of which are properties that are temperature dependent. The properties for fabric numbers 2, 3, 5 and 18 can be seen in Tables A2, A3, A4 and A6, respectively. The properties for air were from Reference [20].

Table 7. Comparison of Measured and Predicted Ignition Times of Front Fabric; GIRCFF Fabric Number 5 Front with Fabric Number 5 Back

GIRCFF Fabric Pairs F	B	Radiant Heat Flux W W/cm^2	Interfabric Spacing G cm	Ignition Time, τ_{ig} Measured s	Predicted s
5	5	6.5	0.0	28.5[1]	17.417[2]
			0.16	22.3[1]	15.110
			0.32	22.9[1]	13.774
			0.64	22.5	12.943
			1.28	34.5	12.422
			1.59	40.75	12.458
			5.0	--	12.961
			10.0	--	13.675
5	none		--	41.0	24.905
5	5	7.6	0.0	22.5[1]	14.340[2]
			0.16	17.5[1]	12.491
			0.32	17.7[1]	11.504
			0.64	17.8	10.943
			1.24	23.0	10.547
			1.59	27.0	10.641
			5.0	--	10.947
			10.0	--	11.463
5	none		--	30.8	13.253
5	5	9.5	0.0	15.1[1]	11.064[2]
			0.16	13.0[1]	9.722
			0.32	12.5[1]	9.091
			0.64	12.6	8.743
			1.28	15.0	8.516

[1] Reference [8]

[2] G = 0.065 cm

Table 7 (concluded)

GIRCFF Fabric Pairs F	B	Radiant Heat Flux W W/cm^2	Interfabric Spacing G cm	Ignition Time, τ_{ig} Measured s	Predicted s
			1.59	17.0	8.531
			5.0	--	8.750
			10.0	--	9.068
5	none		--	16.9	9.996
5	5	13.8	0.0	11.1[1]	7.399[2]
			0.16	8.2[1]	6.639
			0.32	7.5[1]	6.330
			0.64	7.8	6.163
			1.28	8.4	6.053
			1.59	9.0	6.060
			5.0	--	6.163
			10.0	--	6.317
5	none		--	9.6	6.691

[1] Reference [8]

[2] G = 0.065 cm

Table 8. Comparison of Measured and Predicted Ignition Times of Front Fabric; GIRCFF Fabric No. 18 Front and Fabric No. 3 Back

GIRCFF Fabric Pairs F	B	Radiant Heat Flux W W/cm^2	Interfabric Spacing G cm	Destruction Time, τ_{ig} Measured s	Predicted s
18	3	6.8	0.0	26.5	13.066[2]
			0.16	27.0,27.0[1]	9.826
			0.32	26.0,27.0[1]	8.443
			0.64	25.0,28.0[1]	7.796
			1.28	33.0,34.0[1]	7.436
			1.59	40.0,40.0[1]	7.477
			5.0	--	7.946
			10.0	--	8.622
18	none		--	39.8	10.079
18	3	9.0	0.0	26.5	13.066[2]
			0.16	27.0	9.826
			0.32	26.0	8.443
			0.64	25.0	7.796
			1.28	33.0	7.436
			1.59	40.0	7.477
			5.0	--	7.946
			10.0	--	8.622
18	none		--	39.8	10.079

[1] Inside surface of spacers painted black

[2] G = 0.065 cm

Table 8 (concluded)

GIRCFF Fabric Pairs F	B	Radiant Heat Flux W W/cm^2	Interfabric Spacing G cm	Destruction Time, τ_{ig} Measured s	Predicted s
18	3	14.3	0.0	9.6	4.779[2]
			0.16	8.0	3.965
			0.32	8.0	3.702
			0.64	8.1	3.574
			1.28	8.6	3.498
			1.59	8.6	3.506
			5.0	--	3.598
			10.0	--	3.728
18	none			8.6	3.937

[2] G = 0.065 cm

Table 9. Comparison of Measured and Predicted Melting Times of Front Fabric; GIRCFF Fabric Number 2 Front with Fabric Number 5 Back

GIRCFF Fabric		Radiant Heat Flux	Interfabric Spacing	Destruction Time, τ_m	
F	B	W	G	Measured	Predicted
		W/cm^2	cm	s	s
2	5	6.5	0.0	14.0[1]	26.620[2,3]
			0.16	12.2[1]	21.514[2]
			0.32	13.2[1]	16.697[2]
			0.64	17.6	13.063[2]
			1.28	30	10.649[2]
			1.59	40	10.758[2]
			5.0	--	12.722[2]
			10.0	--	15.690[2]
2	none		--	97.5	53.620[2]
2	5	7.6	0.0	10.0[1]	19.721[2,3]
			0.16	9.8[1]	15.754[2]
			0.32	9.5[1]	7.070
			0.64	9.2	5.952
			1.28	33.8	5.342
			1.59	41	5.381
			5.0	--	5.978
			10.0	--	6.989
			--	63.8	10.769

[1] Reference [8]

[2] E = 825 kWs/g mole

[3] G = 0.065 cm

Table 9 (concluded)

GIRCFF Fabric Pairs F	B	Radiant Heat Flux W W/cm^2	Interfabric Spacing G cm	Melting Time, τ_m Measured s	Predicted s
2	5	9.25	0.0	6.4[1]	8.852[2]
			0.16	6.8[1]	6.275
			0.32	6.7[1]	4.967
			0.64	6.8	4.367
			1.28	7.0	4.025
			1.59	9.0	4.045
			5.0	--	4.369
			10.0	--	4.914
2	none		--	21.1	6.159
2	5	13.8	0.0	4.45[1]	5.101[2]
			0.16	4.0[1]	3.564
			0.32	3.7[1]	3.028
			0.64	3.7	2.782
			1.28	4.0	2.633
			1.59	4.0	2.641
			5.0	--	2.771
			10.0	--	2.991
2	none		--	5.2	3.556

[1] Reference [8]

[2] G = 0.065 cm

The kinetic parameters used in the numerical solution are shown in Tables 10, 11, 12 and 13 for fabric numbers 2, 3, 5 and 18, respectively. Acree [8] in his numerical solution for ignition times for fabric number 5 front and fabric number 5 back used for McCarter's data for endothermic pyrolysis [4]. McCarter's value for the activation energy was 219.5 kWs/g mole. This value was experimentally determined using heating rates of 60 C/min [6]. The heating rates encountered in the physical world are of the order of hundreds of C/min. Partly for this reason, an activation energy of 400.0 kWs/g mole was assumed.

The activation energy for endothermic pyrolysis controls the rate of pyrolysis. As seen from equation (4.2), a low value for E means a faster decomposition than what would be achieved with a larger value.

For the front fabric number 5 and rear fabric number 5 combination, with a gap of .32 cm and an intensity of 9.5 W/cm^2, McCarter's value for the endothermic pyrolysis activation energy was used. This value proved to be too low for ignition. With this value, the rate of fabric decomposition is so fast that the mass fraction of pyrolysate at the surface reaches 1.0 before the surface temperature of the front fabric becomes high enough for ignition. With a higher activation energy, the decomposition rate decreases, meaning that more time is required for the pyrolysate concentration at the surface to build up to the point where

Table 10. Reaction Kinetic Parameters, Fabric Number 2 [6]

Moisture Desorption Neglected

Endothermic Pyrolysis, modified kinetics:*

$(\Delta i) = 92.9$ Ws/g

$\varepsilon = 100\%$

$A = 1.04\ (10^{24})1/s$

$n = 0.8$

$E = 363.8$ kWs/g mole

Exothermic reaction neglected

*Discussed in Section 4.6.

Table 11. Reaction Kinetic Parameters, Fabric Number 3 [6]

Moisture Desorption Neglected

Endothermic Pyrolysis

$(\Delta i) = 92.9$ Ws/g

$\varepsilon = 100\%$

$A = 1.04\ (10^{24})$ 1/s

$n = 0.8$

$E = 363.8$ kWs/g mole

Exothermic reaction neglected

Table 12. Reaction Kinetic Parameters, Fabric Number 5 [8]

Moisture Desorption:

$(\Delta i) = 101.6$ Ws/g

$\varepsilon = 5\%$

$A = 4.88 \times 10^{13}$ 1/s

$n = 2.6$

$E = 97.4$ kWs/g mole

Endothermic Pyrolysis, Modified Kinetics:*

$(\Delta i) = 376.8$ Ws/g

$\varepsilon = 90\%$

$A = 9.54 \times 10^{12}$ 1/s

$n = 1.1$

$E = 400$ kWs/g mole

Exothermic Reaction:

$(\Delta i) = 14.78$ kWs/g

$\varepsilon = 5\%$

$A = 9.2 \times 10^{9}$ 1/s

$n = 1.6$

$E = 142.6$ kWs/g mole

*Discussed in Section 4.6.

Table 13. Reaction Kinetic Parameters, Fabric Number 18 [6]

Moisture Desorption:

$(\Delta i) = 101.6$ Ws/g

$\varepsilon = 5\%$

$A = 4.74\ (10^{14})$ 1/s

$n = 2.5$

$E = 104.9 \times 10^{3}$ kWs/g mole

Endothermic Pyrolysis, Modified Kinetics:*

$(\Delta i) = 376.8$ Ws/g

$\varepsilon = 90\%$

$A = 4.98\ (10^{13})$ 1/s

$n = 1.2$

$E = 400$ kWs/g mole

Exothermic Reaction:

$(\Delta i) = 14.78$ kWs/g

$\varepsilon = 5\%$

$A = 2.2\ (10^{11})$ 1/s

$n = 1.2$

$E = 156$ kWs/g mole

*Discussed in Section 4.6.

ignition can be supported. At the same time, this results in higher surface ignition temperatures.

Activation energies of 219.5 kWs/g mole, 340 kWs/g mole, 400 kWs/g mole and 825 kWs/g mole were tried to determine which value would give the best agreement with the experimentally determined values. The value of 219.5 kWs/g mole was tried, but the value was too low to give results. The activation energy of 340 kWs/g mole gave results that were identical to the results obtained using 400 kWs/g mole. The value of 825 kWs/g mole was also used, and the results for values of 400 kWs/g mole and 825 kWs/g mole can be seen in Figure 16. The value of 825 kWs/g mole gave the best agreement with the experimental result. The surface ignition temperatures were ≈840°K at the various gaps. The value of 400 kWs/g mole gave shorter times than the experimental times, and the surface ignition temperatures were ≈720°K. The 400 kWs/g mole is more realistic than the 825 kWs/g mole and the surface temperature is closer to the surface ignition temperature range of 709-715°K previously determined [17]. For this reason, the value of 400 kWs/g mole was used. The predicted destruction times are shown in Figures 17, 18, 19 and 20.

The gap of 0.0 cm is not 0.0 cm but 0.065 as cited in the table. The reason is that for an endothermic activation energy value of 825 kWs/g mole, the best agreement between experimental and predicted ignition times for a gap of 0.0 cm occurred at a gap of 0.065 cm.

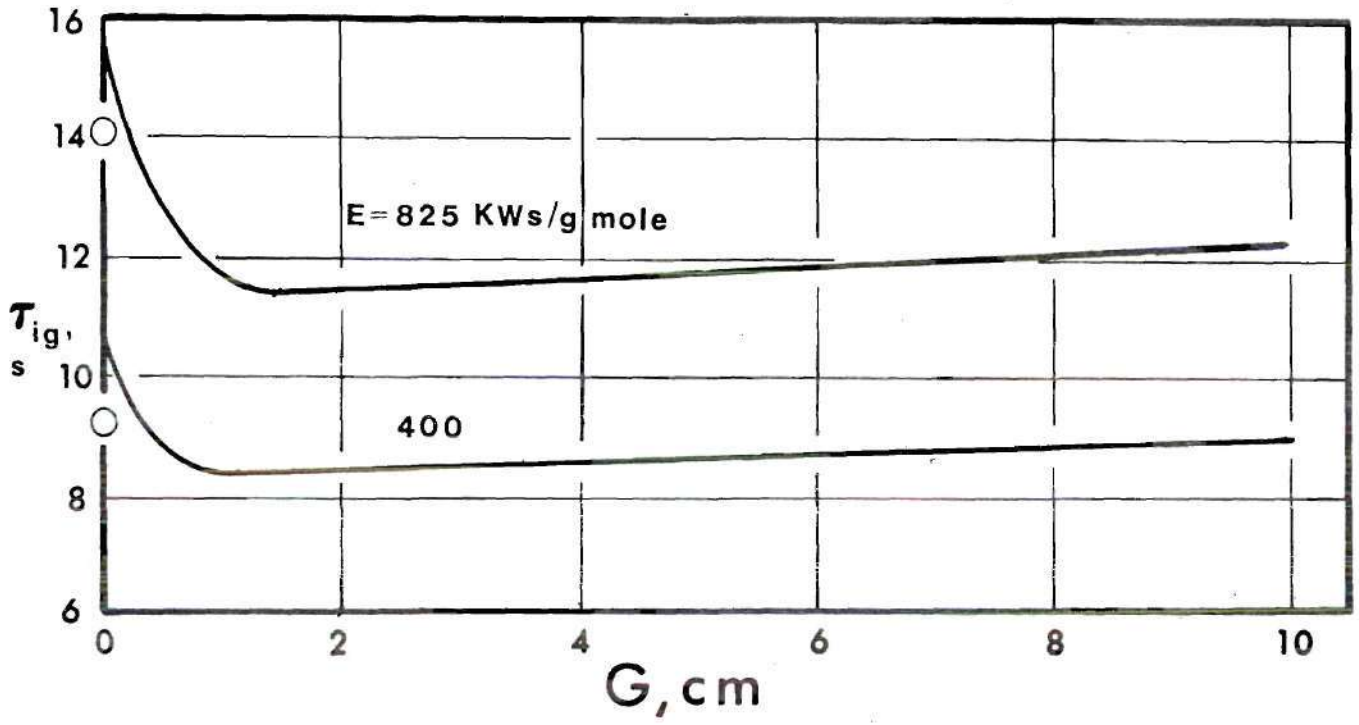

Figure 16. Effect of Activation Energy on Predicted Ignition Time of Front Fabric (GIRCFF Fabric Number 5 Front and Back, W = 9.5 W/cm^2, Open Points Denote Single Predicted Ignition Time)

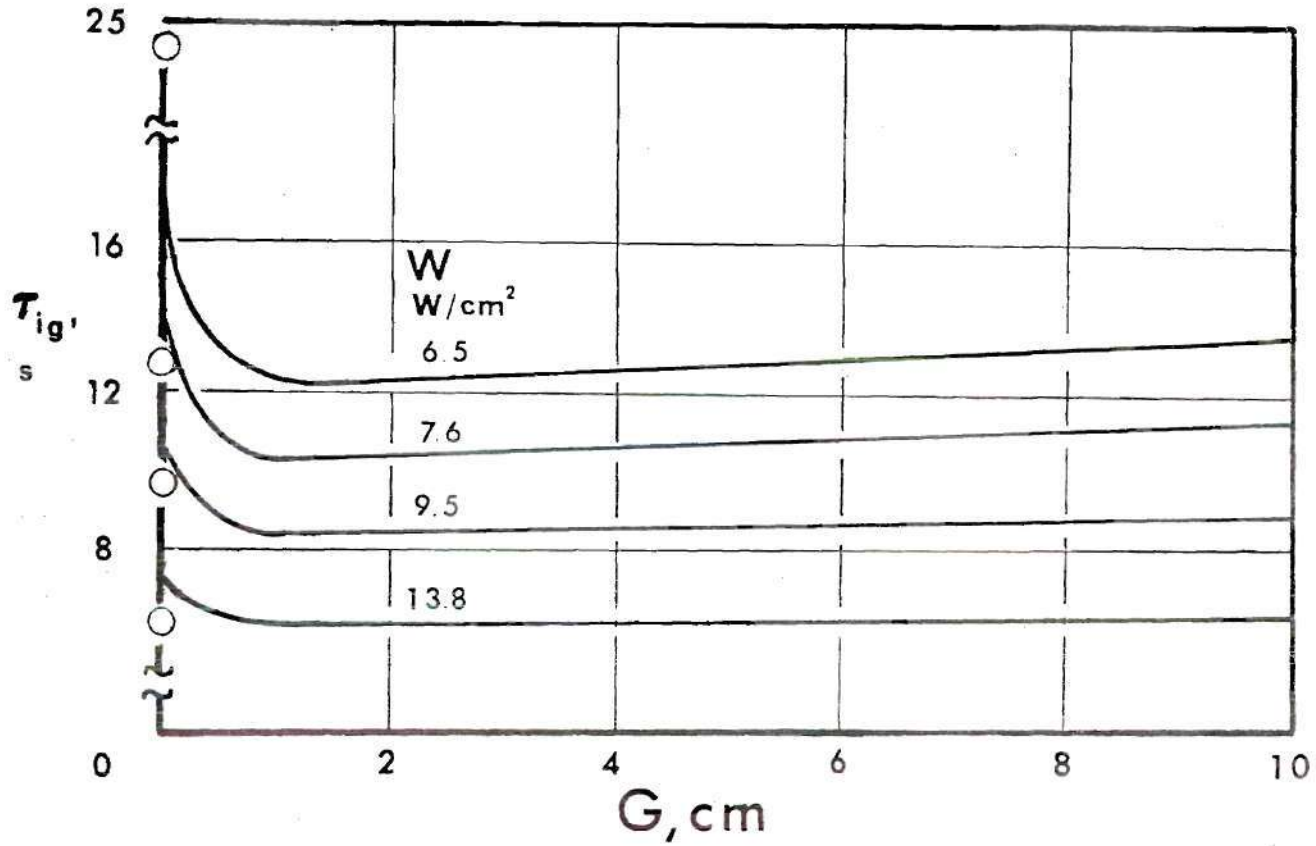

Figure 17. Predicted Ignition Time of the Front Fabric as a Function of Spacing (GIRCFF Fabric Number 5 Front and Back; Open Points Denote Single Fabric Predicted Ignition Time)

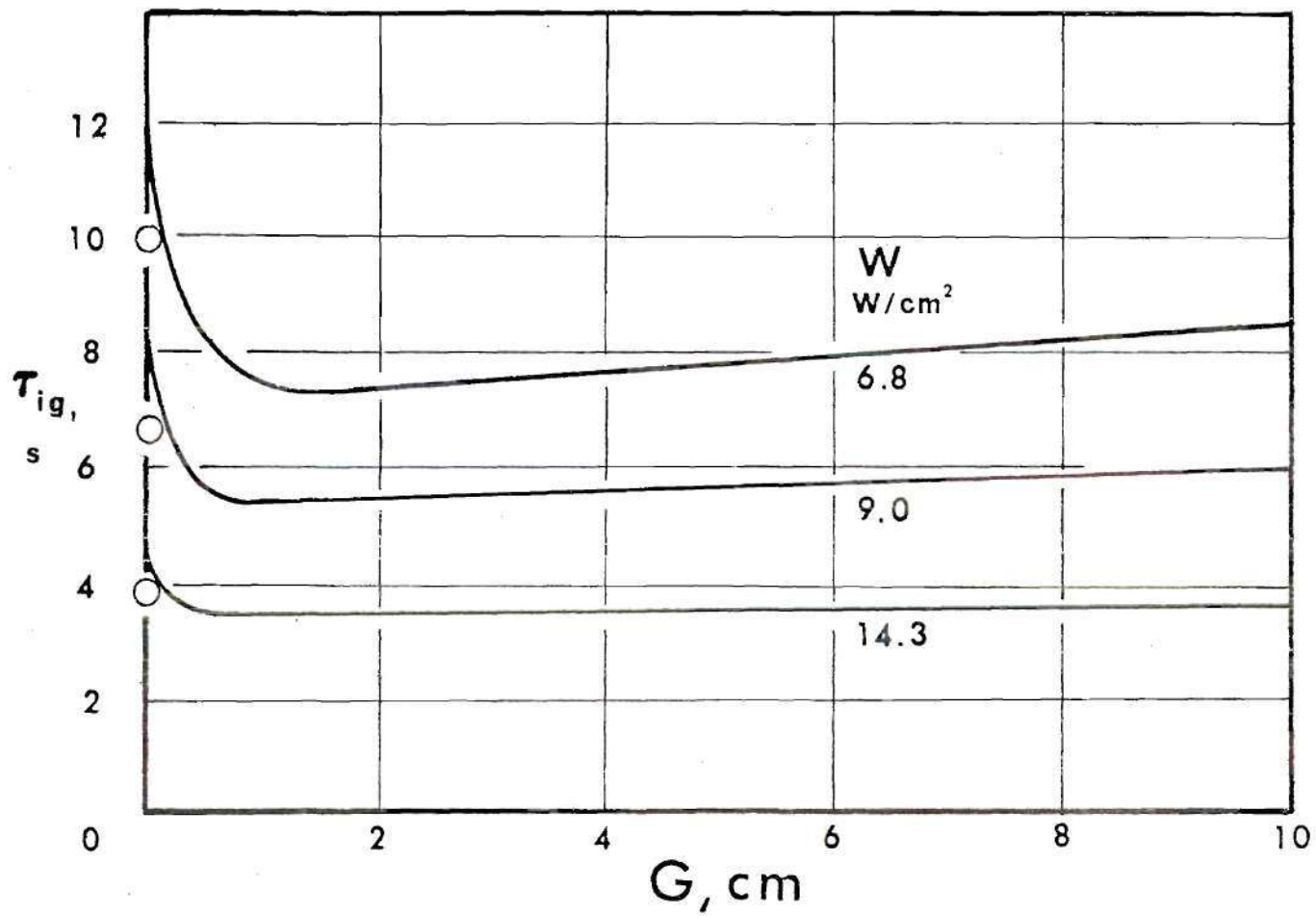

Figure 18. Predicted Ignition Time of the Front Fabric as a Function of Spacing (GIRCFF Fabric Number 18 Front with Fabric Number 3 Back, Open Points Denote Single Fabric Predicted Melting Time)

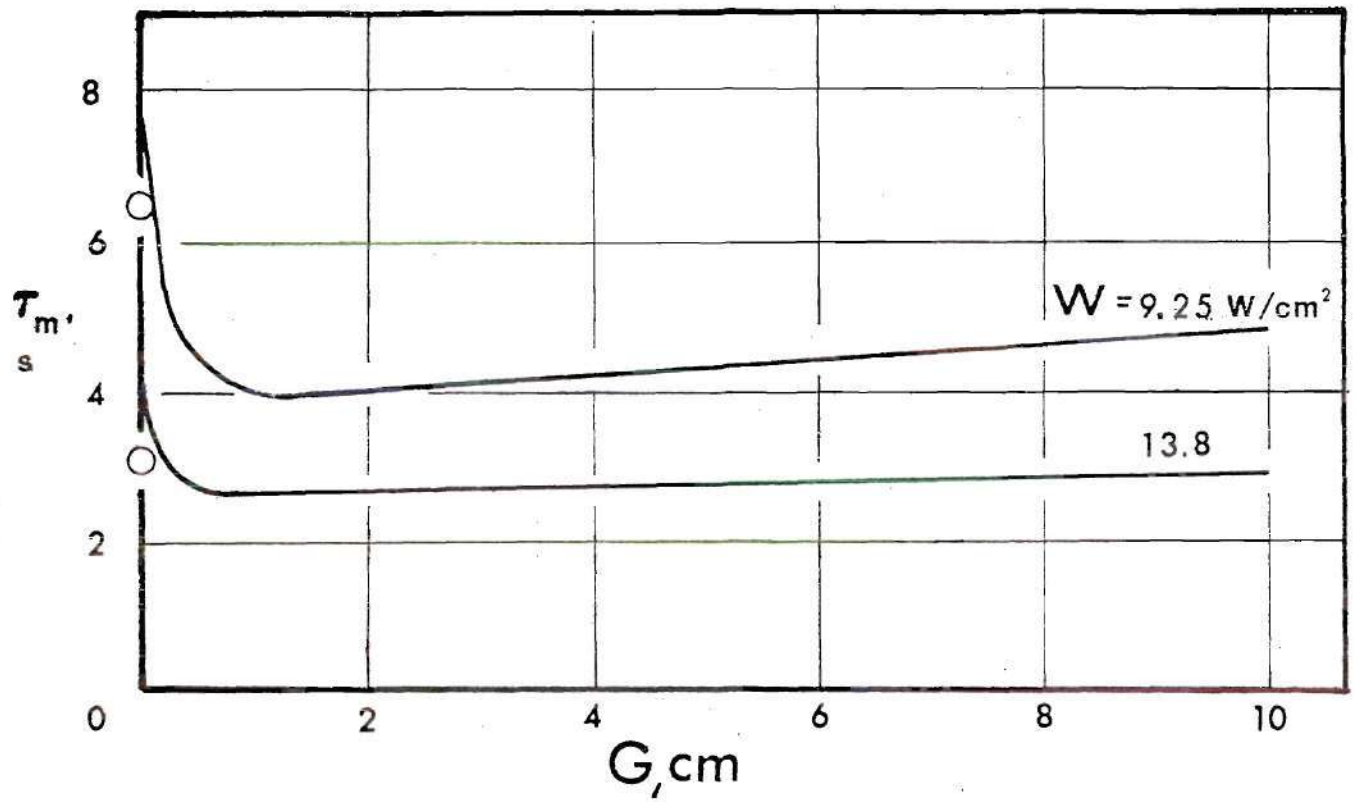

Figure 19. Predicted Melting Time of the Front Fabric as a Function of Spacing (GIRCFF Fabric Number 2 Front with Fabric Number 5 Back, Open Points Denote Single Fabric Predicted Melting Time)

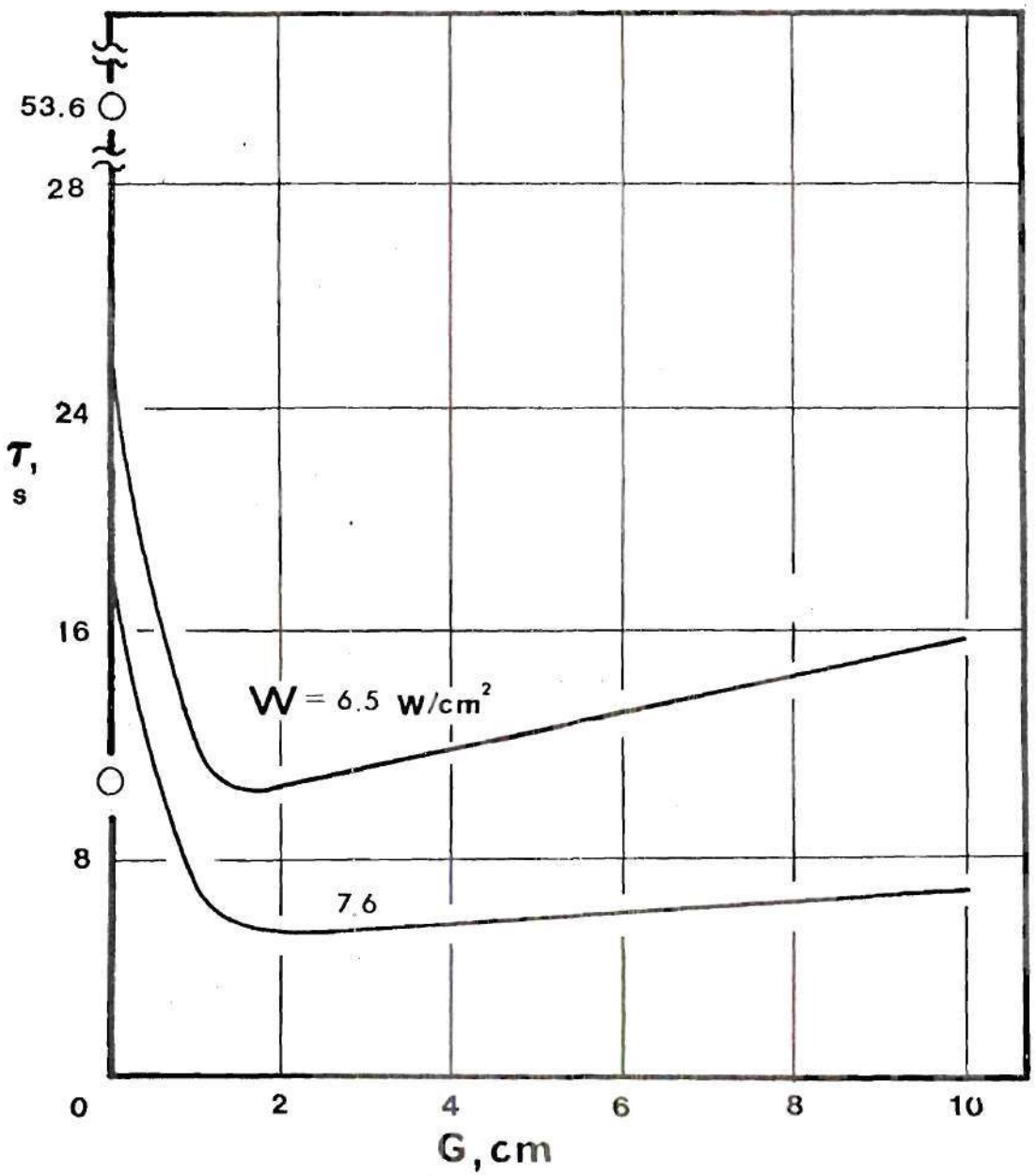

Figure 20. Predicted Melting Time of the Front Fabric as a Function of Spacing (GIRCFF Fabric Number 2 Front with Fabric Number 5 Back, Open Points Designate Single Fabric Predicted Melting Times)

Notice from Tables 7, 8 and 9 that additional gaps of 5 cm and 10 cm were used although no experiments were carried out with such gaps. This was done to show that as the gap increases, the ignition time approaches the ignition time for a single fabric. The point where the effect of convection between the fabric layers becomes more important than conduction occurs at a gap of .64 cm, while the same trend occurred at a .32 cm gap in the experimental results. This transition point is determined by the Grashof number between the fabrics.

The effect of the increased heat transfer between the fabrics due to convection between the fabrics is not as large in the predicted results as in the experimental results. In the actual system, the fabrics are heated and decomposition occurs with corresponding mass injection into the boundary layer. The effect of the mass injection is most pronounced on the heat transfer [24]. This increased heat transfer would increase the ignition times. The effect of mass injection would have a strong effect on the heat transfer between the fabrics as well. With mass injection occurring between the fabrics, it is possible that convective currents within the gaps could be generated, creating an effect much like forced convection in the gap. This could explain why in the actual system the effect of convection between the fabrics is greater than in the predicted times.

The greater the intensity, the closer the predicted times are to the experimental times. With the higher

intensities, the effect of the convective cooling is minimized, thus reducing one source of error.

To simulate the effect of mass injection, the coefficient .59 of equation (4.5) was doubled

$$N_{Nu,L} = 1.18 \ (N_{Gr,x}N_{Pr})^{1/4} \tag{4.66}$$

to simulate the effect of mass injection on the ignition times. The equation was used for the convective losses off the front fabric to the atmosphere. By increasing the convective film coefficient, the heat loss should increase and the ignition time should be longer. By introducing these changes in the model, the ignition time increased from 11.504 sec to 14.159 sec at a gap of .32 cm with an intensity of 7.6 W/cm^2. The fabric combination used was a fabric number 5 front and back. At an intensity of 13.8 W/cm^2 the time increased from 6.330 sec to 6.920 sec.

The properties of the fabrics themselves have a great influence on the ignition time. The predicted ignition time is directly proportional to the specific heat of the front fabric and is inversely proportional to the radiative absorptivity of the front fabric. The radiative absorptivity includes the effects of rereflectivity from the rear fabric. The temperature variable properties helped to increase the ignition time. For example, the specific heat of the fabric increases with temperature, hence this increases the ignition

time.

For the fabric 18 front and 3 back combination, the predicted times were faster than the experimental times. As with the 5 front and 5 back combination, this can be attributed to uncertainty of reaction kinetics and fabric properties and to the mass injection into the boundary layer that occurs in the real system.

The activation energy for pyrolysis used for fabric number 2 was the experimentally determined value. This value predicted melting except for gaps of 0.0 cm and 0.16 cm at an intensity of 7.6 W/cm^2 and for all gaps at an intensity of 6.5 W/cm^2. A value of 825 W/cm^2 was used at these intensities and gaps, and melting was then predicted.

Figure 21 shows the temperature response of fabric number 5 front and back. The front fabric temperature increases initially at a faster rate than the back fabric temperature. After a certain time interval, the temperature response of the front fabric levels off due to pyrolysis and the front and back fabric increase in temperature at the same rate.

Figure 22 shows the boundary layer temperature as a function of boundary layer thickness. The fabric surface temperature is the hottest temperature in the boundary layer. The initial surface temperature is the ambient temperature and increases with time until ignition occurs.

Pyrolysate mass concentration is shown as a function

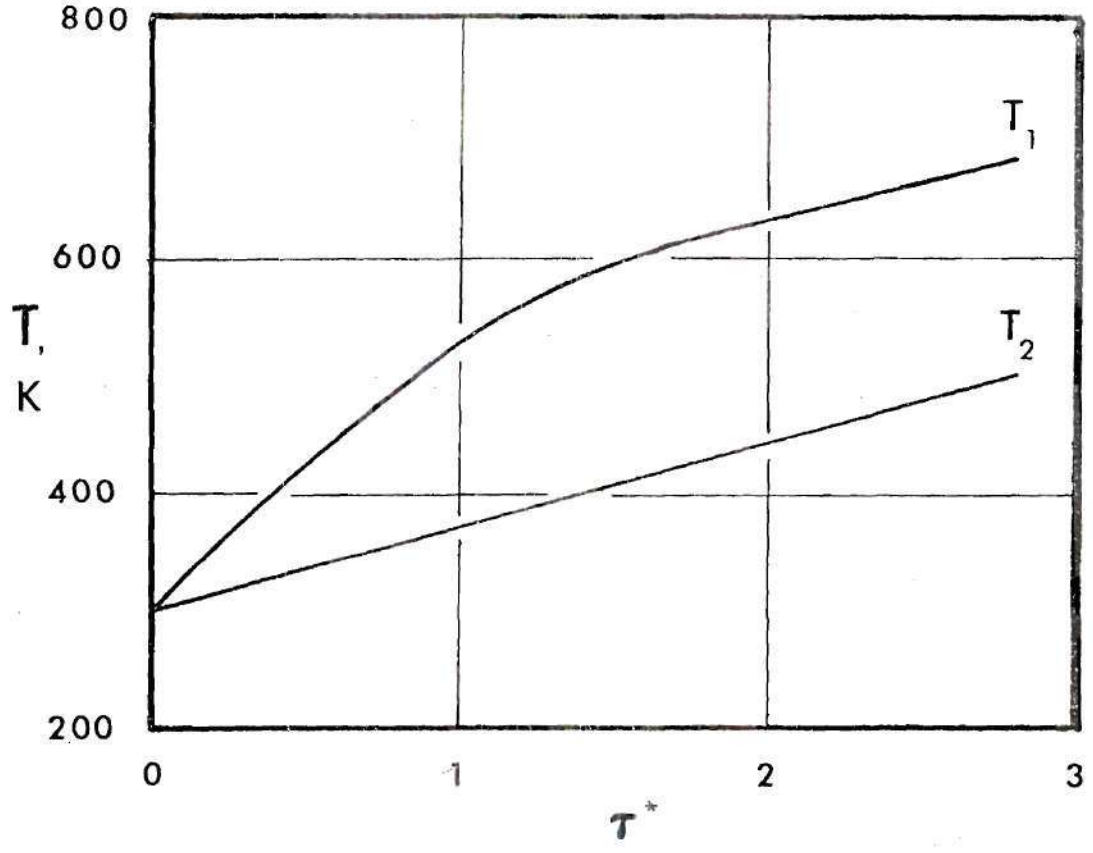

Figure 21. Temperature Response of Front and Back Fabric (GIRCFF Fabric Number 5 Front and Back, W = 6.5 W/cm^2, G = 0.32 cm)

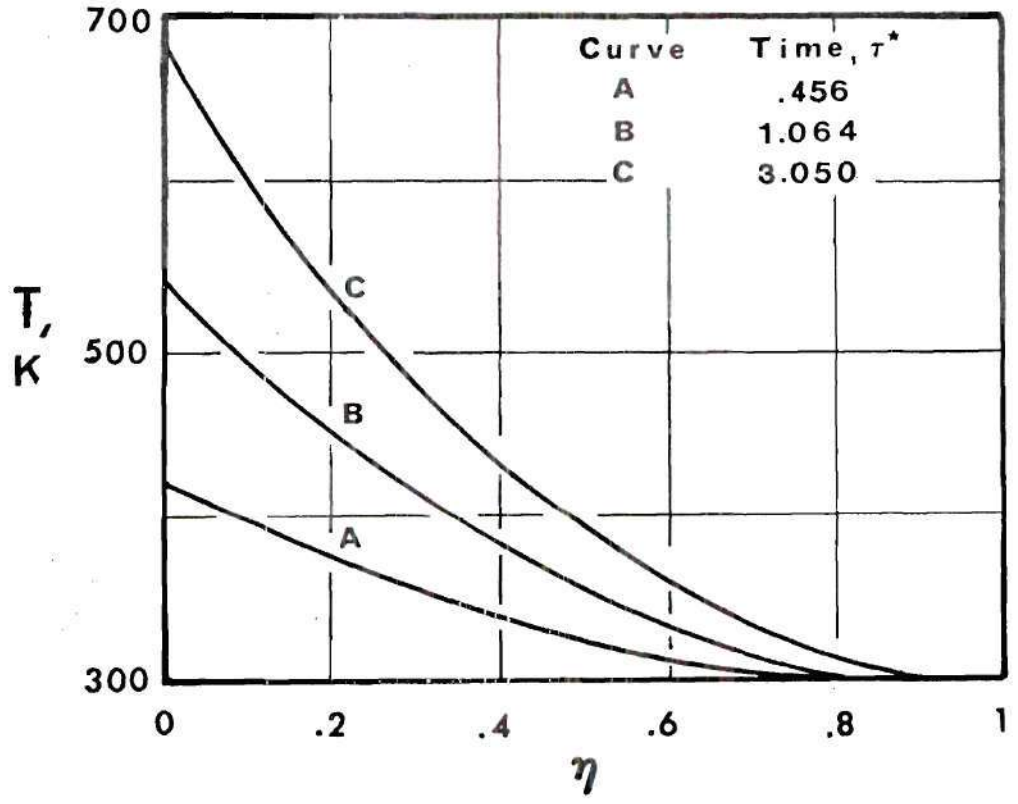

Figure 22. Boundary Layer Temperature Profiles as a Function of Normalized Time (GIRCFF Front Fabric Number Front and Back, W = 6.5 W/cm^2, G = 0.32 cm)

of boundary layer thickness in Figure 23. It is seen that the mass fraction is greater at the fabric surface.

From Figures 22 and 23 it is shown that the fabric surface has the hottest temperature and the richest pyrolysate mass fraction. Ignition was predicted in all cases to occur at the surface and not in the boundary layer. Ignition occurred close to the minimum ignition temperature for a given pyrolysate mass fraction ignition curve and at a lean pyrolysate concentration.

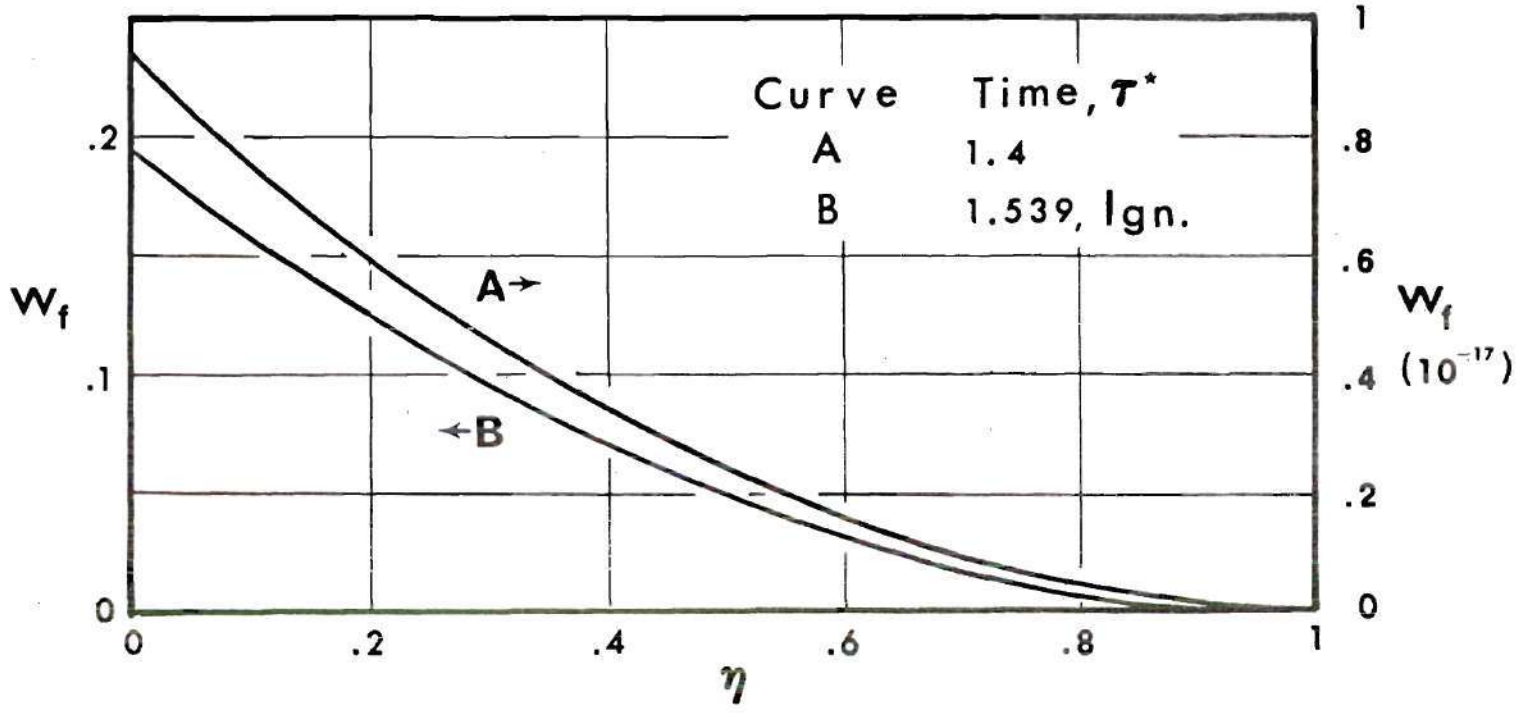

Figure 23. Pyrolysate Mass Fraction Profiles in the Boundary Layer as a Function of Normalized Time (GIRCFF Fabric Number 5 Front and Back, W = 9.5 W/cm^2, G = 0.32 cm)

CHAPTER V

CONCLUSIONS AND RECOMMENDATIONS

The purpose of this research was to investigate the effect of thermal and chemical interactions between fabrics on the ignition time of the front fabric exposed to the heating source. The two tasks studied were first, the investigation of the ignition time of fabric assemblies under convective heating, and secondly, the investigation and the prediction of the ignition time of fabric assemblies under radiative heating.

5.1. Conclusions on Fabric Interaction Under Convective Heating

Ignition time measurements were conducted on horizontal fabric assemblies exposed to a time invariant convective heating source. The tests were designed to examine the effect of heating intensity, gap and fabric porosity on the ignition time of the front fabric. A high and low heating intensity were used. Fabric spacings were set at 0.0, .16 and 1.11 cm. The conclusions on the convective heating of parallel layers are discussed next.

First, the presence of the rear fabric, regardless of its porosity or composition, made no difference on the ignition time of the front fabric. The ignition time

recorded for a fabric assembly was essentially the ignition time of the front fabric alone. Pyrolysate ignition was observed and occurred before solid ignition.

From tests with polyester and cotton fabric pair combinations, no evidence of chemical interaction between fabric layers can be seen.

5.2. Conclusions on Fabric Interaction Under Radiative Heating

Ignition time measurements were conducted on vertical fabric assemblies exposed to a time invariant radiative heating source.

The work of Acree [8] on radiative heating of fabric assemblies was extended to include gaps of .64, 1.28 and 1.59 cm and to include the assembly of fabric number 18 front and 3 back. Incident heat fluxes of 6.5 to 14.3 W/cm^2 were used. The conclusions of the radiant heating of parallel fabric layers are discussed next.

In his work, Acree [8] noted the effect of rereflectivity on ignition time. This effect on the ignition time was investigated further by using increased fabric spacing. It was observed that the effect of the rereflectivity decreases with increased gap. A point is reached where the effect of rereflectivity is negligible and the front fabric ignition time approaches the ignition time of a single fabric. As the gap increases, the effect of convection between the fabrics

increases, thus contributing to the increase in the ignition times.

From a comparison of ignition times of the fabric number 5 front and back combination and the front fabric 18 and back fabric number 3 combination, no significant differences are noted. There is apparent thermal interaction but no evidence of chemical interaction between fabric layers.

An analytical model was developed that incorporates the ignition of the pyrolysate gases in the boundary layer as the ignition criterion. The predicted ignition times were in all instances shorter than the experimental times. The presence of mass injection in the real system and the corresponding greater heat transfer is one reason for the longer experimental times. The correlation equations used in the model for prediction of convective coefficients for the external and internal surfaces are based on free convection with no mass injection.

5.3. Recommendations for Further Work

In order for the developed model to more accurately predict destruction times, further work is needed on the following.

(1) More accurate chemical kinetic values, particularly endothermic pyrolysis activation energies.

(2) Correlation equations for free convection from pyrolyzing solids which include mass injection.

(3) Correlation equations for the heat transfer in the space between two pyrolyzing solids which include mass injection.

It is recommended that the boundary layer ignition criteria be applied to a case where pyrolysis ignition has been observed. One application would be the ignition of a single fabric exposed to convective heating.

This analysis should be modified to take into account the variation of w_f in the x-direction. This analysis assumes a mass fraction profile that is invariant in the x-direction. Experimental results have indicated that the actual point of ignition occurs where $L/2 < x < L$. The analysis should be modified to incorporate the increase in the concentration of w_f as x increases. This would give the x and y coordinates of the point of ignition in the boundary layer.

APPENDIX

Table A1. Property Summary, GIRCFF Fabric No. 1 [6]

1. Description — Fiber Composition: 65/35% Polyester/Cotton
   Color: White
2. Specific Mass — Fabric, $\rho\delta$: 23.49 mg/cm^2
3. Specific Heat

Temperature, T:	323	398	473	K
Specific Heat, c:	1.19	1.34	1.47	Ws/g K

4. Thermal Conductance

Temperature, T:	336.4	381.6	434.6	K
Conductance, k/δ:	15.45	13.31	16.56	W/cm^2 K

5. Infrared Optical Properties

Source	Original		Charred at 219 C
	3160 K	.6-2.5 μm	3160 K
Absorbtivity, $\tilde{\alpha}$	0.184	0.189	0.349
Reflectivity, $\tilde{\rho}$	0.605	0.522	0.366
Transmissivity, $\tilde{\tau}$	0.211	0.289	0.285

6. Reaction Kinetics

	E,kWs/g mole	A, 1/s	n	Δi,Ws/g
Moisture desorption	---	---	---	---
Pyrolysis	365.5	1.28(10^{27})	2.1	28.4
Exothermic reaction	105.4	2.67(10^6)	3.0	---

7. Porosity [25]
   Face exposure: 0.181 (ft/sec)/(lb/ft^2)

Table A2. Property Summary, GIRCFF Fabric No. 2 [6]

1. Description — Fiber Composition: 100% Polyester; Color: Yellow

2. Specific Mass — Fabric, $\rho\delta$: 7.51 mg/cm^2

3. Specific Heat

Temperature, T:	322	398	473	K
Specific Heat, c:	1.42	1.42	1.42	Ws/g-K

4. Thermal Conductance

Temperature, T:	371	366	422.6	K
Conductance, k/δ:	20.3	21.0	22.8	W/cm^2 K

5. Infrared Optical Properties

Source	Original		Charred at 219 C
	3160°K	.6-2.5 μm	3160 K
Absorbtivity, $\tilde{\alpha}$:	.164	.153	.175
Reflectivity, $\tilde{\rho}$:	.560	.501	.582
Transmissivity, $\tilde{\tau}$:	.276	.346	.243

6. Reaction Kinetics

	E, kWs/g mole	A, 1/s	n	Δi, Ws/g
Moisture desorp.	---	---	---	---
Pyrolysis	363.8	1.04×10^{24}	1.7	389.0
Exothermic react	---	---	---	---

7. Porosity [25]

Face exposure: 0.70 (ft/sec)/(lb/ft^2)

Table A3. Property Summary, GIRCFF Fabric No. 3 [6]

1. Description — Fiber Composition: 100% Polyester
   Color: White
2. Specific Mass — Fabric, $\rho\delta$: 20.91 mg/cm^2
3. Specific Heat

Temperature, T:	323	398	473	K
Specific Heat, c:	1.03	1.25	1.67	Ws/g K

4. Thermal Conductance

Temperature, T:	336.2	382.7	434.0	K
Conductance, k/δ:	5.40	5.54	6.29	W/cm^2 K

5. Infrared Optical Properties

Source	Original		Charred at 219 C
	3160°K	.6-2.5 μm	3160 K
Absorptivity, $\tilde{\alpha}$:	.190	.143	.200
Reflectivity, $\tilde{\rho}$:	.560	.619	.506
Transmissivity, $\tilde{\tau}$:	.250	.276	.306

6. Reaction Kinetics

	E, kWs/g mole	A, 1/s	n	Δi, Ws/g
Moisture desorp.	---	---	---	---
Pyrolysis	363.8	1.04x10^{24}	0.8	92.9
Exothermic reaction	---	---	---	---

7. Porosity [25]
   Face exposure: 5.1 (ft/sec)/(lb/ft^2)

Table A4. Property Summary, GIRCFF Fabric No. 5 [8]

1. Description — Fiber Composition: 100% Cotton; Color: White

2. Specific Mass — Fabric, $\rho\delta$: 13.71 mg/cm^2

3. Specific Heat

Temperature, T:	323	398	473	K
Specific Heat, c:	1.05	1.47	1.91	Ws/g

4. Thermal Conductance

Temperature, T:	343.9	403.5	479	K
Conductance, k/δ:	7.32	8.81	10.82	$W/cm^2°K$

5. Infrared Optical Properties

Source	Original		Charred at 219 C
	3160°K	.6-2.5 μm	3160 K
Absorptivity, $\tilde{\alpha}$:	.179	.183	.225
Reflectivity, $\tilde{\rho}$:	.533	.521	.491
Transmissivity, $\tilde{\tau}$:	.288	.296	.284

6. Reaction Kinetics

	E,kWs/g mole	A,1/s	n	Δi,Ws/g
Moisture desorption	97.4	4.88×10^{13}	2.6	101.6
Pyrolysis	219.5	9.54×10^{12}	1.1	376.8
Exothermic reaction	142.6	9.20×10^{19}	1.6	14780.0

7. Porosity [25]

Face exposure: 1.18 (ft/sec)(lb/ft^2)

Table A5. Property Summary, GIRCFF Fabric No. 17 [6]

1. Description — Fiber Composition: 65/35% Polyester/Cotton
   Color: White
2. Specific Mass — Fabric, $\rho\delta$: 8.55 mg/cm^2
3. Specific Heat

Temperature, T:	323	398	473	K
Specific Heat, c:	1.27	1.47	1.66	Ws/g K

4. Thermal Conductance

Temperature, T:	345.6	391	472.3	K
Conductance, k/δ:	17.34	22.48	26.75	W/cm^2 K

5. Infrared Optical Properties

Source	Original		Charred at 219 C
	3100°K	.6-2.5 μm	3160 K
Absorptivity, $\tilde{\alpha}$:	0.151	0.164	0.425
Reflectivity, $\tilde{\rho}$:	0.485	0.464	0.255
Transmissivity, $\tilde{\tau}$:	0.364	0.372	0.320

6. Reaction Kinetics

	E,kWs/g mole	A,1/s	n	Δi,Ws/g
Moisture desorption	---	---	---	---
Pyrolysis	310.3	1.80(10^{19})	1.6	28.4
Exothermic reaction	105.4	2.67(10^6)	3.0	---

7. Porosity [25]
   Face exposure: 1.89 (ft/sec)(lb/ft^2)

Table A6. Property Summary, GIRCFF Fabric No. 18 [6]

1. Description — Fiber Composition: 100% Cotton; Color: White

2. Specific Mass — Fabric, $\rho\delta$: 12.88 mg/cm^2

3. Specific Heat

Temperature, T:	323	398	473	K
Specific Heat, c:	1.44	1.63	1.82	Ws/g K

4. Thermal Conductance

Temperature, T:	346	407.4	478.3	K
Conductance, k/δ:	5.55	6.72	8.74	W/cm^2 K

5. Infrared Optical Properties

Source	Original		Charred at 219 C
	3160°K	.6-2.5 μm	3160 K
Absorptivity, $\tilde{\alpha}$:	.170	.176	.241
Reflectivity, $\tilde{\rho}$:	.599	.573	.527
Transmissivity, $\tilde{\tau}$:	.231	.251	.232

6. Reaction Kinetics

	E, kWs/g mole	A, 1/s	n	Δi, Ws/g
Moisture desorp.	104.9	$4.74(10^{14})$	2.5	101.6
Pyrolysis	229.6	$4.98(10^{13})$	1.2	376.8
Exothermic reaction	156.0	$2.2(10^{11})$	1.2	14780.0

7. Porosity [25]

Face exposure: 1.19 (ft/sec)(lb/ft^2)

School of Mechanical Engineering
Fire Hazard and Combustion Research Laboratory

IGNITION TIME OF FABRICS
CITA

Date: 5-11-76 Experiment No.: 66 Experimentor: RL
Fabric No.: 17 Fabric Holder Aperture: 63.5 mm
Fabric Inclination Angle: 0 Fabric Height Above Burner: 10.5cm
Room Temperature: 23.3 C Barometric Pressure: 29.21" Hg
Room Relative Humidity: 59%

	Flow Meter			
Gas	P(" Hg)	T (mV)	T (°F)	R(Div)
Methane	12.4			142.5
Air	5.4			82

Flame Temperature: _____ mV _____ °C

Oscilloscope Settings

Upper Beam

Sensitivity: 10 V/cm

Lower Beam

Sensitivity: 10 mV/cm
Sweep Rate: .5 s/cm

Infrascope

Scale: A
Emissivity: 1

Ignition Time:

4.0 cm; 2.0 s

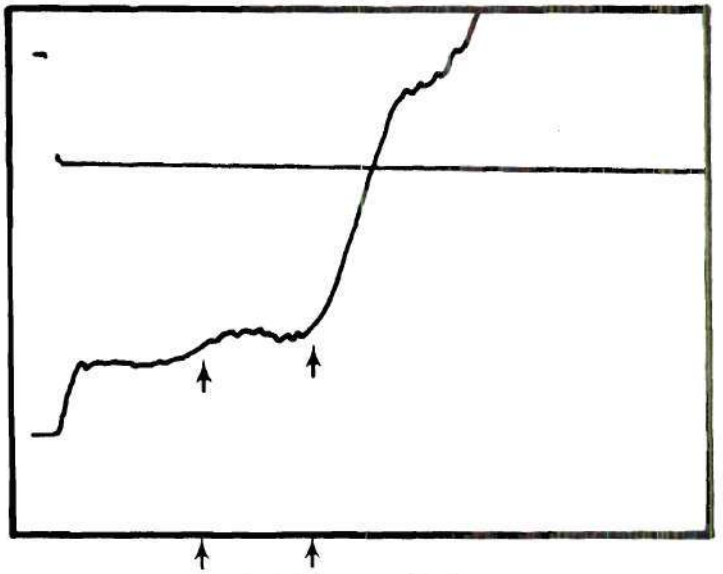

Solid Ignition

Pyrolysate Ignition

Figure B1. Sample Fabric Assembly Ignition Time Test-CITA

School of Mechanical Engineering
Fire Hazard and Combustion Research Laboratory

FABRIC ASSEMBLY IGNITION TIME TEST
RITA

Test No. 279

Date 5-25-76

Experimentors RL

Remarks

GIRCFF FABRIC NO.:

Front 5 Back 5

IRRADIATION:

Idle Voltage 80 V

Incident Heat Flux (W_o) 7.6 W/cm^2

Relative Humidity 25 %

Spacing Between Fabrics 1.59 cm

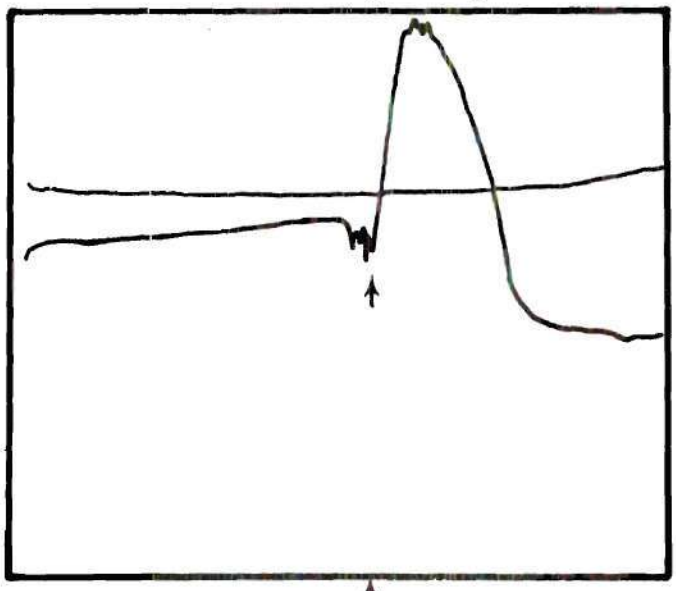

Ignition

U.B. Sensitivity 500 mV/cm T

L.B. Sensitivity 10 mV/cm MI

Sweep Rate 5 s/cm

INFRASCOPE READING:

Temperature Scale Setting MI(A), T(blk)

Emissivity MI(1), T(1)

Ignition Time 5.4 cm

Ignition Time 27.0 s

Figure B2. Sample Fabric Assembly Ignition Time Test-RITA

School of Mechanical Engineering
Fire Hazard and Combustion Research Laboratory

FABRIC ASSEMBLY IGNITION TIME TEST
RITA

Test No. 220

Date 2-17-76

Experimentors RL

Remarks _____

GIRCFF FABRIC NO.:

Front 2 Back 5

IRRADIATION:

Idle Voltage 80 V

Incident Heat Flux (W_o) 7.6 W/cm^2

Relative Humidity 30 %

Spacing Between Fabrics .64 cm

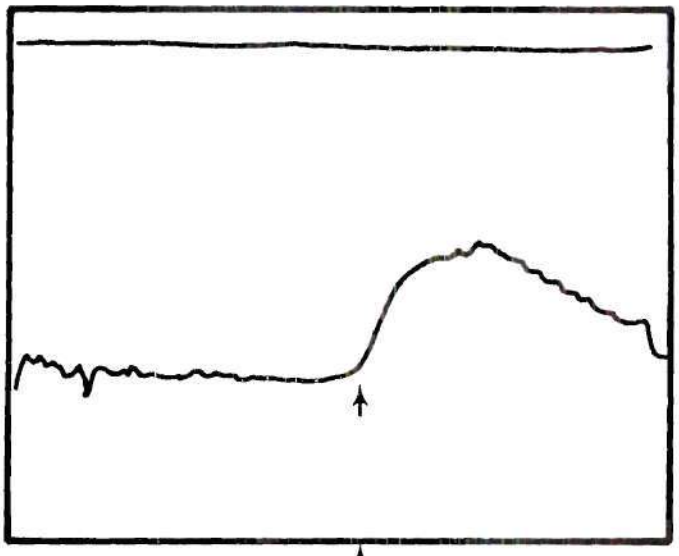

Melting

U.B. Sensitivity --- mV/cm ____

L.B. Sensitivity 10 mV/cm MKI

Sweep Rate 2 s/cm

INFRASCOPE READING:

Temperature Scale Setting B

Emissivity 1

Ignition Time 5 cm

Ignition Time 10 s

Figure B3. Sample Fabric Assembly Melting Time Test-RITA

BIBLIOGRAPHY

1. "America Burning," The Report of the National Commission on Fire Prevention and Control, Superintendent of Documents, U. S. Government Printing Office, Washington, D. C. 20402, GPO Bookstore Stock No. 5200-00004 (1973).

2. "Flammable Fabrics," Fourth Annual Report, U. S. Department of Health, Education and Welfare, Superintendent of Documents, U. S. Government Printing Office, Washington, D. C. 20402, (1972).

3. Evans, R. B., Wulff, W. and Zuber, N., "The Study of Hazards from Burning Apparel and the Relation of Hazards to Test Methods," Research Proposal Submitted by the School of Mechanical Engineering, Georgia Institute of Technology, to the Government-Industry Research Committee on Fabric Flammability, Office of Flammable Fabrics, NBS, Washington, D. C. 20234, July 1970.

4. Alkidas, A., Hess, R. W., Wulff, W. and Zuber, N., "Study of Hazards from Burning Apparel and the Relation of Hazards to Test Methods," Final Report, NSF Grant No. GK-27189, School of Mechanical Engineering, Georgia Institute of Technology, Atlanta, Georgia, (1971), National Technical Information Access No. COM-73-10954.

5. The Government-Industry Research Committee on Fabric Flammability, "Study of Hazards from Burning Apparel and the Relation of Hazards to Test Methods," a Work Statement Prepared by the Research Committee, Dr. E. Passaglia, Chairman, National Bureau of Standards, June, 1970.

6. Durbetaki, P., Wulff, W., et al., "Study of Hazards from Burning Apparel and the Relation of Hazards to Test Methods," Second Annual Report, NSF (RANN) Grant No. GI-31882, School of Mechanical Engineering, Georgia Institute of Technology, Atlanta, Georgia (1972), NTIS Access No. PB-242-597/AS.

7. Durbetaki, P., Wulff, W., et al., "Fabric Ignition," Third Annual Report, NSF (RANN) Grant No. GI-31882, School of Mechanical Engineering, Georgia Institute of Technology, Atlanta, Georgia, (1974), NTIS Access No. PB-242-740/AS.

8. Acree, R. L., "Ignition Time Measurements on Fabric Assemblies Under Various Geometric Configurations," M.S. Thesis, School of Mechanical Engineering, Georgia Institute of Technology, Atlanta, Georgia, (1974).

9. Miller, B., "The Thermal and Flammability Behavior of Multicomponent Fibrous Polymer Systems," NSF Grant No. GI-37805, a Progress Report Presented at the NSF/RANN Conference on Fire Research, Georgia Institute of Technology, Atlanta, Georgia, May, 1974.

10. Wulff, W. and Durbetaki, P., "Fabric Ignition and the Burn Injury Hazard," Heat Transfer in Flames, N. H. Afgan and J. M. Beer, editors, Scripta Book Company, Washington, D. C. (1974), pp. 451-461.

11. Tribus, M., "Decision Analysis: Approach to Satisfying the Requirements of the Flammable Fabrics Act," Paper presented at the Textile and Needles Trades Division, American Society of Quality Control, Greensboro, N. C., February 12, 1970.

12. Steward, F. R., "Ignition Characteristics of Cellulosic Materials," Heat Transfer in Fires, P. L. Blackshear, editor, Scripta Book Co., Washington, D. C. (1974), pp. 379-407.

13. Kanury, A. M., "Ignition of Cellulosic Solids--A Review," Fire Research Abstracts & Reviews, National Academy of Sciences, 14, (1972), pp. 24-52.

14. Merzhanov, A. G. and Averson, A. E., "The Present State of the Thermal Ignition Theory: An Invited Review," Combustion and Flame, 16, (1971), pp. 89-124.

15. Annamalai, K. and Durbetaki, P., "Ignition of Thermally Thin Porous Pyrolyzing Solids Under Normally Impinging Flames," Combustion and Flame, 27, (1976), pp. 253-266.

16. Wulff, W., "Ignition of Pyrolyzing Solids," School of Mechanical Engineering, Georgia Institute of Technology, Atlanta, Georgia, unpublished results, 1974.

17. Durbetaki, P., Annamalai, K. and Matson, G. L., and Ryszytiwskyj, W. P., "Prediction of Fire Hazard in Buildings," Fourth Annual Report, NSF Grant No. GI-31882, School of Mechanical Engineering, Georgia Institute of Technology, Atlanta, Georgia, December, 1975.

18. Champion, E. R., "Determination of Fabric Ignition Times Through Use of a Convective Heat Source Apparatus," M.S. Thesis, School of Mechanical Engineering, Georgia Institute of Technology, Atlanta, Georgia, (1973).

19. Durbetaki, P., Lloyd, L. R. and Tincher, W. C., "Ignition Probability of Thermally Thin Materials Subject to Convective Heating: Effect of Orientation," Symposium on Flammabilities and Combustion of Non-Metallic Materials, 172nd National Meeting of the American Chemical Society, San Francisco, California, September, 1976.

20. Kreith, F., Principles of Heat Transfer, 3rd Edition, Intext Educational Publishers, New York (1973).

21. Eckert, E. R. G. and Drake, R. M., Analysis of Heat and Mass Transfer, McGraw-Hill Book Company, New York, 1972, p. 780.

22. Jakob, M., Heat Transfer, Volume I, John Wiley and Sons, Inc., New York, 1949, pp. 534-539.

23. Tingle, W. J., "Effects of Heating Rate of Pyrolyzing Materials on Ignition Characteristics of Pyrolysate-Air Mixtures," M.S. Thesis in progress, School of Mechanical Engineering, Georgia Institute of Technology, Atlanta, Georgia, January, 1976.

24. Eichhorn, R., "The Effect of Mass Transfer on Free Convection," Journal of Heat Transfer, ASME, Series C, 82, (1960), pp. 260-263.

25. Wedel, G. L., "Determination of Convective Film Coefficients under Simulated Pyrolysate Evolution," M.S. Thesis, School of Mechanical Engineering, Georgia Institute of Technology, Atlanta, Georgia, August, 1974.